Journal of Materials Chemistry C

REVIEW

View Article Online
View Journal | View Issue

Check for updates

Cite this: J. Mater. Chem. C, 2018, 6, 3815

Recent advances in the fabrication of graphene–ZnO heterojunctions for optoelectronic device applications

Feng-Xia Liang,[a] Yang Gao,[b] Chao Xie,[c] Xiao-Wei Tong,[c] Zhong-Jun Li*[c] and Lin-Bao Luo*[c]

Received 11th January 2018,
Accepted 19th February 2018

DOI: 10.1039/c8tc00172c

rsc.li/materials-c

Recently, by taking advantage of the synergistic effects of both graphene and ZnO, various photoelectric devices that combine graphene and ZnO have exhibited excellent device performances and attracted increasing research interest. However, although significant achievements have been made, many challenges still exist. In this review paper, we comprehensively summarize the recent advances in the fabrication of various graphene (also including reduced graphene oxide)–ZnO (*e.g.* ZnO films, nanowires, nanotubes, nanorods *etc.*) hybrid heterostructures, and their application in a number of optoelectronic devices, including photodiodes, phototransistors, solar cells, light emitting diodes (LEDs), lasers and so on. We start by briefly surveying the recent progress in the fabrication methodologies such as low-temperature and high-temperature methods. And then, we will elaborate on the optoelectronic device application in terms of device physics, performance analysis, and device optimization approaches. Finally, we close with some unresolved issues and challenges in this field.

Published on 19 February 2018. Downloaded by HeFei University of Technology on 20/04/2018 03:48:02.

1. Introduction

ZnO is an important II–VI compound semiconductor material with a wide direct band gap (3.37 eV) and high exciton binding energy (60 meV) at room temperature.[1,2] Due to their excellent properties in optics and electrical transport,[3] ZnO nanostructures, in particular one-dimensional ZnO nanostructures (1D ZnO, *e.g.* nanowires, nanorods, nanotubes, *etc.*), have found wide application in various electronic devices such as field effect transistors (FETs),[4,5]

[a] School of Materials Science and Engineering and Anhui Provincial Key Laboratory of Advanced Functional Materials and Devices, Hefei University of Technology, Hefei, Anhui 230009, China
[b] Institute of Industry and Equipment Technology, Hefei University of Technology, Hefei 230009, Anhui, China
[c] School of Electronic Sciences and Applied Physics, Hefei University of Technology, Hefei, Anhui 230009, China. E-mail: zjli@hfut.edu.cn, luolb@hfut.edu.cn

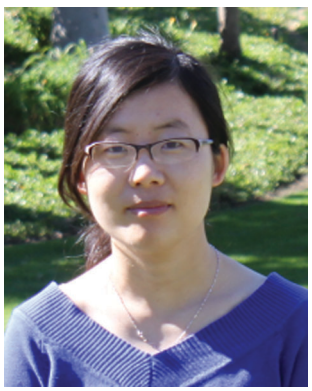

Feng-Xia Liang

Feng-Xia Liang, received her BS degree from Liaocheng University, MS degree from University of Science and Technology of China, and PhD degree from City University of Hong Kong, in 2003, 2006 and 2012, respectively. She is currently an associate professor in the School of Materials Science and Engineering at Hefei University of Technology. Her research interest includes the synthesis of low-dimensional semiconductor nanostructures for chemical, biological and optoelectronic devices applications.

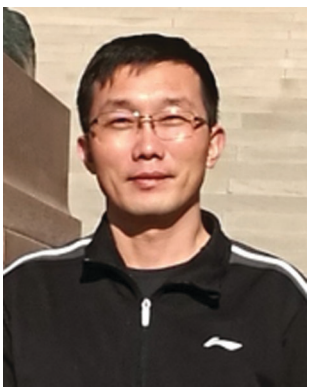

Zhong-Jun Li

Zhong-jun Li, earned his BS degree from the Department of Physics at Anhui Normal University in 2000. He achieved his PhD degree from Department of Modern Physics, at University of Science and Technology of China in 2008, majoring Atomic & Molecular Physics. After graduation, he then joined the School of Electronic Science & Applied Physics of Hefei University of Technology, and is currently an associate professor. His research interests include the simulation and manipulation of electronic structures of low-dimension semiconductor materials and their applications in devices.

Published on 19 February 2018. Downloaded by HeFei University of Technology on 20/04/2018 03:48:02.

chemical or gas sensors,[6,7] non-volatile memory devices,[8] and piezoelectric nanogenerators.[9,10] In addition, in the past decade, substantial efforts have been devoted to the development of various ZnO-based optoelectronic devices such as solar cells,[11,12] light-emitting diodes (LEDs),[13,14] ultraviolet photodetectors (UVPDs) and lasers.[15,16]

Graphene is another pivotal material that has a typical two-dimensional geometry with a single layer of carbon arranged in a honeycomb structure. It has drawn global research interest in the past decade due to its excellent properties, such as ultra-high carrier mobility (200 000 cm^2 V^{-1} s^{-1}), excellent optical transparency, chemical and mechanical stability and good mechanical strength and elasticity.[17–19] These beneficial characteristics along with the tunable electrical and optical properties and good compatibility of graphene with the modern Si-based technologies[20] render graphene a promising building block for assembling various photonic and optoelectronic devices and systems that can afford multiple functions of signal emitting, transmitting, modulating, and detection.[21] In spite of these numerous progresses, it is undeniable that graphene-based devices have their own shortcomings.[22–24] Because of the short light–matter interaction length, the intrinsic low optical absorption of only 2.3% for single-layer graphene is insufficient for light-harvesting device applications.[25] On the other hand, the ultra-short lifetime of excitons in pure graphene causes fast carrier recombination, which is detrimental to the generation of photocurrent or photovoltage.[26] The emergence of graphene–semiconductor hybrid heterostructures provides a feasible solution to the above dilemma in that the hybrid structure can profit from the synergistic characteristics of both materials.[27,28] Taking graphene–ZnO based photodiodes for example, when graphene is in contact with ZnO, a built-in electric field will be formed at the graphene–ZnO interface due to the difference in work functions between the graphene and ZnO. Once illuminated by UV light with an energy larger than the band gap of ZnO, the ZnO will absorb photons and the resultant photo-generated electron–hole pairs will be efficiently separated by the electric field, forming a photocurrent in the external circuit. In comparison with conventional photodetectors solely composed of ZnO material, the graphene–ZnO hybrid photodiode is characterized by the following three features:[29,30] (1) fast response speed. Owing to the built-in electric field, the photo-generated electron–hole pairs can be efficiently separated, leading to a relatively fast response speed; (2) large responsivity and detectivity. Because of the rectifying behavior, the current under dark conditions is much lower than other photoconductive-type photodetectors, which is beneficial for high responsivity and detectivity; (3) low energy consumption. Like conventional metal–semiconductor (M–S) Schottky junction, the graphene–ZnO heterojunction often exhibits typical photovoltaic behavior, which allows the heterojunction to act as a self-driven photodetector without an external power supply. Besides photodiode application, the graphene–ZnO heterostructures have also proved to be ideal building blocks for assembling other optoelectronic devices including phototransistors, solar cells, LEDs, lasers, and waveguides.[31,32] In order to gain a straightforward insight into applications of graphene–ZnO hybrid structures, some representative optoelectronic devices are summarized in Fig. 1.

In this paper, we will review recent progress in the fabrication of graphene–ZnO (*e.g.* ZnO thin films, nanowires, nanotubes, nanorods *etc.*) hybrid heterostructures using either low-temperature or high-temperature methods. This is followed by discussing the applications of graphene–ZnO hybrid structures in a number of optoelectronic devices, including photodiodes, phototransistors, solar cells, light emitting diodes (LEDs), lasers and so on. In the final section, conclusions of the existing techniques are presented and future challenges in optoelectronic applications of graphene–semiconductor hybrid heterostructures are also proposed.

Lin-Bao Luo

Lin-Bao Luo is a full professor of applied physics at Hefei University of Technology. He received his MSc in inorganic chemistry at Department of Chemistry, University of Science and Technology of China, and PhD degree in 2009 from Department of Physics and Materials Sciences, City University of Hong Kong. He joined the Hefei University of Technology in 2011. He has published more than 110 peer reviewed journals with a total citation of ~3000 and an H-index of 30. His research interest mainly focuses on the controlled fabrication of one-dimensional semiconductor nanostructures for optoelectronic and electronic devices applications including photovoltaic devices, photodetector, and non-volatile memory device.

2. Fabrication of graphene–ZnO hybrid heterojunction

The most convenient way to achieve a graphene–ZnO heterojunction is to simply transfer a large-area graphene sheet onto the surface of ZnO *via* an aqueous transfer process after separate synthesis of both materials.[33] The graphene is grown at 1000 °C by using a mixed gas of CH_4 and H_2 *via* a chemical vapor deposition (CVD) method in which Cu foils were used as the catalytic substrates. After growth, the graphene was spin-coated with 5 wt% polymethylmethacrylate (PMMA) in chlorobenzene, and then the underlying Cu foils were removed using a marbles's reagent solution. In a typical transfer process, the ZnO was usually first cleaned with alcohol and acetone under ultrasonication. Afterwards, the ZnO was soaked in deionized water, and then slowly lifted to mount the graphene onto ZnO. In fact, such an aqueous transfer method has been widely utilized to obtain other van der Waals graphene–semiconductor (*e.g.*, Ga_2O_3, Si, GaAs and so on) heterojunctions.[34–36] On the other hand, a number of synthetic techniques such as CVD, electro-chemical deposition method, hydrothermal method, metal–organic vapor-phase

 This journal is © The Royal Society of Chemistry 2018

Published on 19 February 2018. Downloaded by HeFei University of Technology on 20/04/2018 03:48:02.

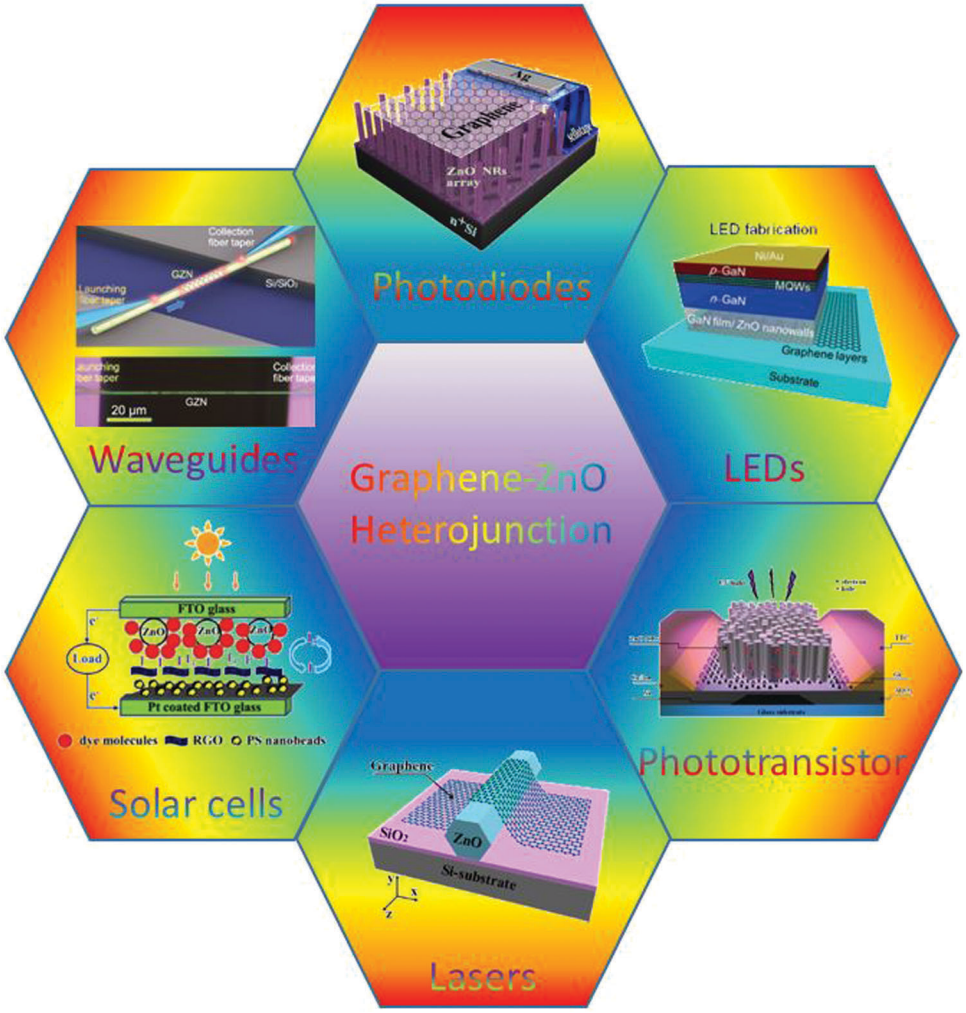

Fig. 1 Schematic illustration of the graphene–ZnO heterojunction for various optoelectronic device applications.

epitaxy (MOVPE), pulsed laser deposition (PLD), *etc.*, have also been developed to grow ZnO thin film or nanostructures directly on graphene. Generally, these methods can be classified into two groups: low-temperature methods (*e.g.*, hydrothermal process, electrodeposition, *etc.*) and high-temperature methods (*e.g.*, CVD, MOVPE, and PLD). Liu's group reported the synthesis of ZnO nanorod arrays with high optical qualities on few-layer graphene sheets by using zinc nitrate hexahydrate and hexamethylenetetramine as precursors under hydrothermal conditions (Fig. 1).[37] It was observed that the dimensions, density as well as morphology of the ZnO nanostructures can be readily tailored by changing the growth conditions, such as the temperature, reagent concentration and pH values. Further photoluminescence and cathodoluminescience spectra revealed strong near-band-edge emission, which confirms the high optical quality of the as-synthesized nanostructures. In fact, under similar mild conditions, ZnO nanoparticles and nanowire arrays can also be combined with graphene oxide to form ZnO–graphene oxide nano-composites, which found important applications in photodetectors from the visible to near-infrared range,[38] and photocatalytic reaction.[39,40] Electrochemical deposition that has advantages including simplicity, low cost, and rapid growth at a low temperature, has also become a popular method for the synthesis of ZnO nanostructures on graphene.[41,42] For example, dense and vertical ZnO nanotubes (NTs) have been successfully grown on graphene using a seedless electrochemical deposition method in pure zinc nitrate solution.[43] The electrochemical growth of ZnO nanotubes on graphene film was performed in a three-electrode cell at 90 °C using a saturated calomel electrode (SCE), graphite sheet and graphene on glass as the reference, counter, and working electrodes, respectively. During the electrochemical growth, the electrolyte solution (0.01 M $Zn(NO_3)_2$) was kept stable without stirring and current density (*vs.* the SCE reference electrode) was kept at -0.5 mA cm^{-2} for 3 hours (Fig. 2).

Compared with the above low-temperature methods, the ZnO obtained from high-temperature processing is often characterized by high-quality crystallinity with a relatively low density of defects and good transport properties. For this reason, high-temperature methods are more frequently used to fabricate high-quality graphene–ZnO heterojunctions for optoelectronic device applications.[44,45] As an example, CVD proved to be a promising route to synthesize 1D ZnO nanostructure arrays

Published on 19 February 2018. Downloaded by HeFei University of Technology on 20/04/2018 03:48:02.

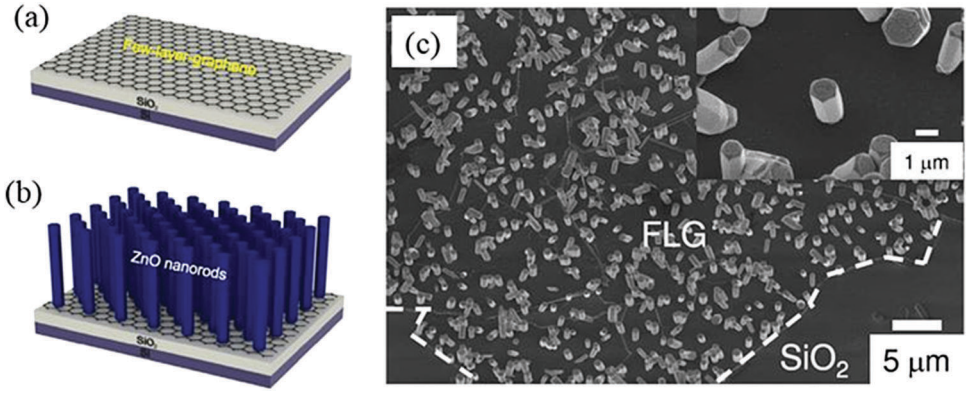

Fig. 2 Schematic illustration of the fabrication process. (a) Transfer of graphene on SiO_2/Si substrates, (b) growth of ZnO nanostructures on graphene through a hydrothermal process, and (c) SEM image of the ZnO nanorods on graphene. Reproduced with permission from Kim *et al.*, *Nanotechnology*, 2011, **22**, 245603. Copyright 2011 Institute of Physics.

(*e.g.*, nanorods,[46] and nanowires[47,48]) onto graphene layers, which was usually carried out in a tube furnace by oxidizing metallic Zn powder. The growth temperature was kept in the range from 450 to 900 °C. MOVPE represents another popular high-temperature method that has been widely adopted to grow ZnO on a graphene surface.[49] Yi's group has successfully grown free-standing ZnO nanostructure arrays on graphene sheets with gaseous diethylzinc as the precursor. In their work, the structures of ZnO (aspect ratio, density, morphology) were observed to strongly depend on the growth temperature. Furthermore, the formation of aligned ZnO nanoneedles in a row and vertically aligned nanowalls was observed and explained in terms of enhanced nucleation on graphene step edges and kinks.

ZnO in many different nanoscale forms can be easily grown without much effort.[50,51] It will bring about a native point defect (*e.g.*, surface defects, Zn interstitials, and oxygen vacancy) during the growth process.[52,53] Various studies have shown that these defects can lead to not only n-type conductivity of ZnO but also exhibit very strong blue or green emissions, which allow various novel devices to be achieved. Even though the characterization and origin of these defects in ZnO is still a question of debate, it has been widely observed from both experiment and theoretical simulation that O vacancies are deep donors, Zn interstitials are too mobile to be stable at room temperature. In addition, the famous green luminescence has several possible reasons, such as Cu impurities and Zn vacancies. This means precise control of its rich defect chemistry is of paramount importantance for achieving high performance optoelectronic devices, in particular solid-state white lighting devices.[54]

3. Graphene–ZnO hybrid structure photodetectors

3.1 Graphene–ZnO photodiodes

Thanks to the large surface-to-volume ratio and unique opto-electronic properties, low-dimensional ZnO nanostructures (*e.g.*, NRs, NWs, quantum dots (DQs)) are highly preferable for ultraviolet photodetection application.[55–57] Compared with a device solely composed of ZnO nanostructures, graphene–ZnO heterojunction photodetectors including photodiodes and phototransistors can take advantage of the synergistic benefits from both materials,[58,59] and therefore they usually exhibit high responsivity, high specific detectivity, high photoconductive gain, and low energy consumption.[60,61] It is worth noting that the sensitivity of the graphene–ZnO UVPD could be optimized when ultrathin AlO_x film was introduced between the graphene and ZnO wafer by electron beam evaporation.[62] Remarkably, after the interfacial passivation, the dark current decreased a little bit from 2.8×10^{-4} to 2.38×10^{4} A; however, the photocurrent was considerably increased from 5.85×10^{-4} to 2.89×10^{-3} A, leading to an increase in the on/off ratio from 2.1 to 12.1. Reasonably, this increase in sensitivity is due to effective suppression of recombination activities at the ZnO surface, as a result of reduced density of surface dangling bonds and defect after interfacial passivation with an AlO_x ultrathin layer.

Nie *et al.* reported the first graphene–ZnO photodiode by simply coating undoped free-standing ZnO nanorod arrays with a layer of graphene film that was derived using a CVD method (Fig. 3a).[33] Theoretical simulation results revealed that such a graphene–ZnO photodiode exhibited excellent light absorption, due to the strong light trapping effect, as indicated by Fig. 3b. This special optical characteristics allow the device to monitor pulsed ultraviolet light illumination with a frequency as high as 2250 Hz, and the fall/rise times were measured to be 0.7/3.6 ms, respectively. In addition, the responsivity and photoconductive gain of this UV photodiode were estimated to be 113 A W^{-1} and 385 at a bias of −1 V, respectively (Fig. 3c–e). By replacing the above undoped ZnO nanorods with an Al-doped ZnO nanorod array, a high-performance self-powered UV light photodetector exhibiting a UV-to-visible rejection ratio of 1×10^{2}, and a short rise time of 37 μs was developed. In order to eliminate the intrinsic defects such as oxygen vacancy or zinc interstitial, which may cause a response peak in the visible region, Duan *et al.* utilized a surface treatment in an oxygen-rich environment to passivate the ZnO nanorods. It was observed from the PL spectrum that after surface treatment, the sample indeed exhibited a near-band-edge emission peak at 380 nm, and an

 This journal is © The Royal Society of Chemistry 2018

Published on 19 February 2018. Downloaded by HeFei University of Technology on 20/04/2018 03:48:02.

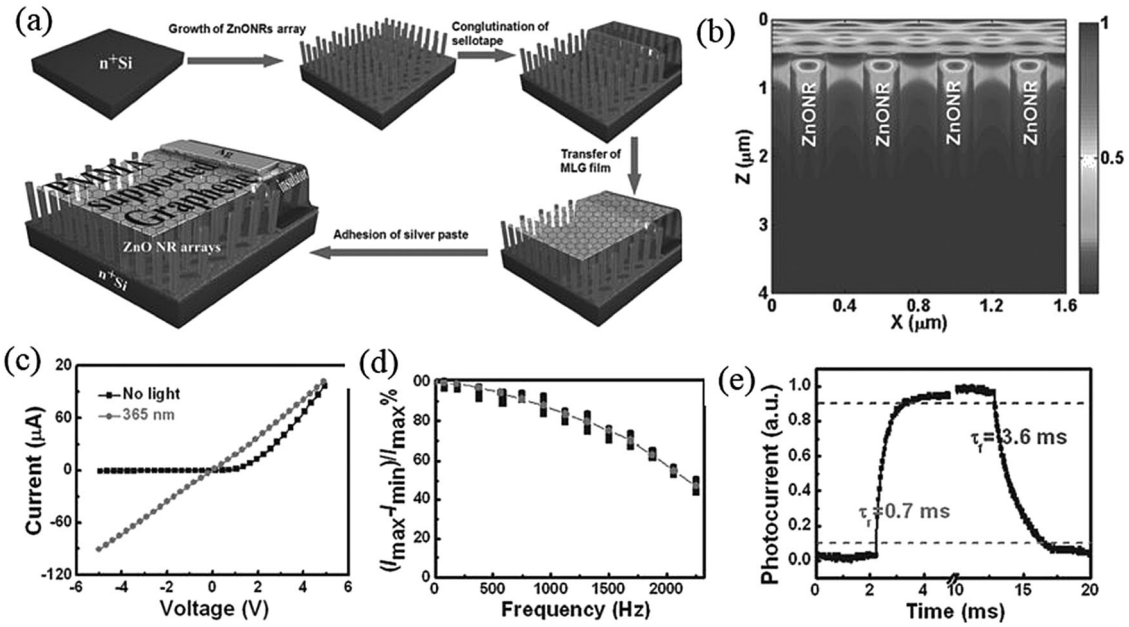

Fig. 3 (a) Schematic illustration of the fabrication of the graphene–ZnO NWs array UV photodiode. (b) Simulated electric field energy density distribution of the photodiode at 365 nm illumination. (c) *I–V* curves of the photodiode in the dark and under 365 nm illumination. (d) Relative balance of the UV photodiode as a function of different frequencies. (e) A single normalized cycle for estimating the rise time and fall time. Reproduced with permission from Nie *et al.*, *Small*, 2013, **9**, 2872. Copyright 2013 Wiley.

optimized spectral selectivity.[63] Wu's group developed a seedless solution process for controllable growth of crystalline ZnO micro/nanowires on single-layer graphene sheets.[64] The alignment of the ZnO micro/nanowire correlated well with the density of the wires, which was determined by the sample configuration in solution and the graphene surface cleaning. UV photodetectors based on the vertically aligned ZnO on graphene displayed a high responsivity of 1.62 A W^{-1} per volt. Such a value is a 500% improvement over epitaxial ZnO devices, a 300% improvement over ZnO nanoparticle devices, and a 40% improvement over the previous best results for nanowire/graphene hybrid devices.

Sandwiching a single ZnO NW between two graphene layers can lead to sensitive UV light photodetectors as well.[65] The on–off ratio of the as-sandwiched UV device was as high as 8×10^2 at a bias of 3 V, with a rise time of 0.7 s, which is much better than the device solely assembled from ZnO NW. This relatively good device performance is not only ascribed to the existence of the Schottky barrier between the graphene and ZnO NW, but also to the larger light absorption efficiency and effectual interface area than other ZnO-based Schottky barrier UV detectors using metal electrodes.[66] Later on, a more sensitive UV photodetector was achieved when a free-standing ZnO NW array was sandwiched by two graphene layers.[67] The as-assembled structure allows the NW array to be in direct contact with the graphene layers, minimizing the effect of the substrate or metal electrodes. Optoelectronic analysis revealed that the as-sandwiched graphene–ZnO NW array–graphene heterostructures demonstrated a high sensitivity and excellent photo-elastic response under UV illumination along with a faster response and recovery time.

Reduced graphene oxide (rGO) with promising optical and electrical properties offers the potential for cost-effective and large-scale production, and thereby it is also an ideal building block for assembling hybrid heterojunction UV devices.[68] For instance, Liu *et al.* reported an rGO film/ZnO NW hybrid device through electrophoretic deposition of rGO sheets on the top of ZnO NW arrays.[69] It was found that the hybrid devices exhibited a fast and greatly enhanced broadband photovoltaic response that resulted from the formation of interfacial Schottky junctions between ZnO and rGO. In order to optimize the device performance of the UV photodiode, Dhar *et al.* tried to sensitize a ZnO NRs/PEDOT:PSS hybrid heterojunction with graphene QDs (GQDs), a new type of zero dimensional material with strong optical absorption, and unique size-dependent optical and electrical properties.[70] These devices possessed a fast photodetection speed along with a higher responsivity and external quantum efficiency (EQE). Furthermore, the photodetectors could keep the responsivity under low light conditions, with the response spectrum extended to the near infrared (NIR) region.

For the above graphene–ZnO based devices, the interface, in particular the barrier height of the Schottky junction virtually plays a very important role during the photosensing process.[71,72] In this sense, modulation *via* a strain-induced piezotronic effect has become a popular approach to tailor the optoelectronic process, where the generation, separation, and recombination of electron–hole pairs can be efficiently tuned by the piezopotential.[73] For example, Zhang's group developed a strain modulation approach in an effort to improve the photoelectric conversion efficiency.[74] It was unveiled that under a compressive strain of 0.349%, 17% enhancement in photosensing property was realized. Such an increase in photoresponse, according to

Published on 19 February 2018. Downloaded by HeFei University of Technology on 20/04/2018 03:48:02.

the energy band theory and simulation result, is related to higher Schottky barrier height and widened depletion region, which are induced by the piezoelectric field (Fig. 4).

Even though the integration of graphene with ZnO is beneficial for UV light photodiode applications, it is undeniable that the carrier transfer between graphene and the semiconductor will decrease the barrier height of the diode, which limits the performance improvement of the graphene–semiconductor UV photodiode. To overcome this issue, Wu *et al.* introduced an insulating h-BN layer into a graphene–ZnO Schottky junction.[75] The resultant graphene/h-BN/ZnO hybrid structure exhibited an enhanced rectifying behavior and very high UV photoresponse, with a responsivity as high as 1350 A W^{-1}. Such an optimization in photoresponse is mainly related to the introduction of an insulating h-BN layer that can act as a tunneling layer for holes produced in the ZnO and a blocking layer for holes in the graphene (Table 1).

3.2 Graphene–ZnO phototransistors

Graphene–ZnO UV light phototransistors are geometrically characterized by two metal electrodes on the graphene layer, which suggests a completely different operation mechanism from the photodiode.[76] Under UV light illumination, the graphene will act as a carrier transport channel, while the ZnO is used as the photo absorbing material.[77,78] Although a built-in electric field is also formed at the graphene–ZnO interface, it is nevertheless not used to separate the photo-generated electron–hole pairs, as often in graphene–ZnO UV photodiodes. Dang *et al.* reported a hybrid channel UV phototransistor composed of graphene–ZnO NW arrays, which was capable of detecting both photocurrent and photovoltage (Fig. 5a).[79] Device analysis revealed that the phototransistor had a high sensitivity and selectivity towards the near UV region (Fig. 5a). Additionally, the device could work at a low voltage and show good reproducibility, and high responsivity and photoconductive gain (Fig. 5c). Flexible and sensitive graphene–ZnO NW hybrid UV phototransistors were also successfully assembled on polyethylene terephthalate (PET) substrates.[80] From the negative shift of the Dirac point in the transfer characteristics, the responsivity was calculated to be 3×10^8 V W^{-1}, which can be ascribed to the transfer of electrons from ZnO to graphene with a transferred electron concentration of 6×10^{12} electrons per mW cm^{-2}. Remarkably, the flexible graphene–ZnO hybrid phototransistor had excellent device stability, even after 10 000 cycles of bending at a strain of 0.5%.

Similarly, highly dense ZnO NW arrays could be grown onto graphene structures including three-dimensional graphene foam and rGO to form sensitive UV light phototransistors.[81,82] For instance, by using a resistive thermal evaporation technique, Boruah *et al.* fabricated a ZnO NWs–graphene foam hybrid structure that showed an excellent UV photoresponse, with fast response and recovery times of 9.5 and 38 s, respectively, and an EQE as high as 2490.8%. The photosensitivity of the device could

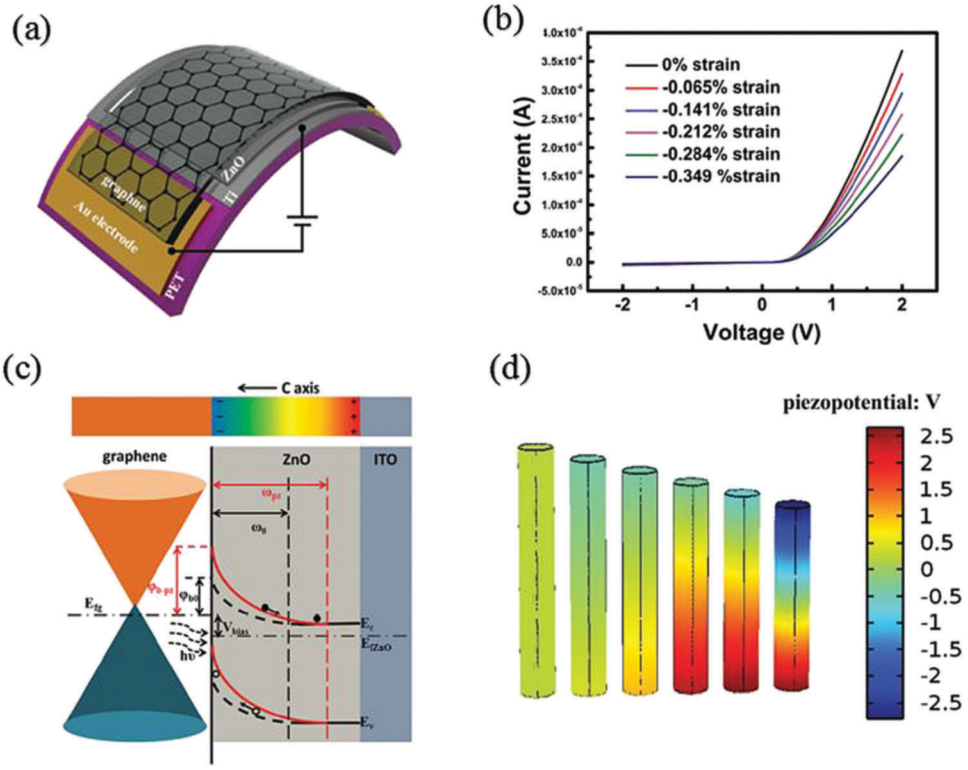

Fig. 4 (a) Schematic illustration of a graphene–ZnO UV photodiode. (b) *I*–*V* curves of the graphene–ZnO UV photodiode under different compressive strains. (c) Schematic band diagrams of the graphene–ZnO UV photodiode with compressive strain. (d) Theoretical simulation of the pizeoelectronic potential distribution in the ZnO NWs under different strains. Reproduced with permission from Liu *et al.*, *Adv. Funct. Mater.*, 2016, **26**, 1347–1353. Copyright 2016 Wiley.

 This journal is © The Royal Society of Chemistry 2018

Published on 19 February 2018. Downloaded by HeFei University of Technology on 20/04/2018 03:48:02.

Table 1 Comparison of device performance of various graphene–ZnO heterojunction based photodetectors. The PD, PT, and CO in brackets denote photodiode, phototransistor, and composite respectively

Device geometries	On/off ratio	Response speed	Responsivity (A W^{-1})	Detectivity (Jones)	Ref.
Gr–ZnONW (PD)	10^3	3.6 ms	113	—	33
rGO–ZnONW (PD)	2	0.11 s	0.55 (mV W^{-1})	—	38
Gr–ZnO film (PD)	10^4	280 μs	0.5	3.9×10^{13}	58
Gr–ZnO film (PD)	10^2	—	—	—	60
Gr–ZnO wafer (PD)	12.1	<1 s	3.0×10^4	4.33×10^{14}	61
Gr–ZnO QDs (PD)	230	14 ms	247	—	62
Gr–ZnO:Al NW (PD)	10^2	37 μs	5×10^{-4}	750	63
Gr–ZnONW–Gr (PD)	800	0.7 s	—	—	65
Gr–ZnONW–Gr (PD)	—	3	23	—	66
GrQDs–ZnONW–polymer (PD)	—	—	36	1.3×10^{12}	70
Gr–ZnONW (PD)	—	<1 s	85	—	74
Gr–hBN–ZnO (PD)	3	<5 s	1350	—	75
Gr–ZnONW (PT)	1.30	3.2	3×10^5	—	79
Gr–ZnONW (PT)	1.25	10 s	2.5×10^6	—	80
Gr foam–ZnONW (PT)	2	9.5 s	8		81
rGo–ZnO NW (PT)	5	0.1	—	—	83
Gr–ZnOQDs (CO)	1.1×10^4	2	—	—	86
Gr–ZnOQD (PT)	—	—	1.1×10^8	5.1×10^{13}	90
Gr–ZnOQD (PT)	1.7	5	9.9×10^8	7.5×10^{14}	91
Gr–ZnOQD (PT)	500	1000	1.7×10^3	—	92

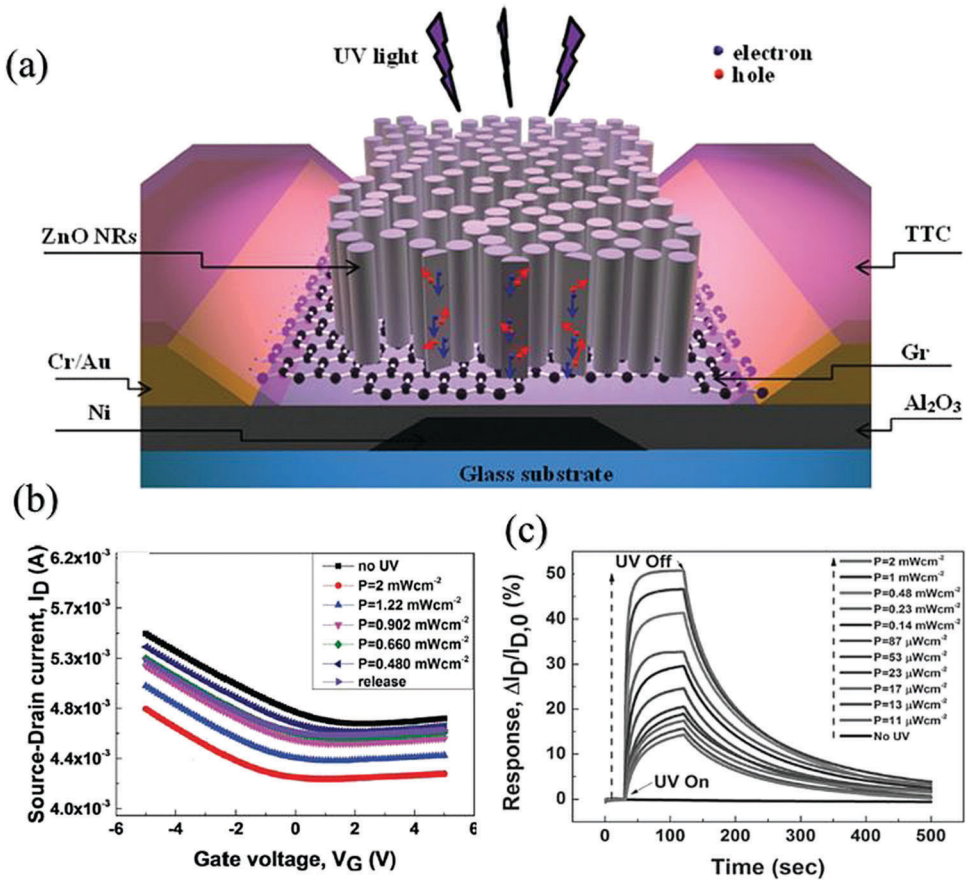

Fig. 5 (a) Schematic of a graphene–ZnO UV phototransistor. (b) Transfer characteristics of the graphene–ZnO UV phototransistor under UV illumination with different intensities. (c) Photoresponse of the graphene–ZnO UV phototransistor at a bias voltage of 1 V. Reproduced with permission from Dang *et al.*, *Small*, 2015, **25**, 3054–3065. Copyright 2015 Wiley.

be understood as follows: under UV illumination, electron–hole pairs were produced with an energy higher than or equal to the bandgap of the ZnO and caused desorption of oxygen molecules for trapping of generated free holes by oxygen ions present on the surface. A decrease in the depletion layer led to an increase in free charge carrier concentrations, which increases the conductivity of

Published on 19 February 2018. Downloaded by HeFei University of Technology on 20/04/2018 03:48:02.

the device. Yang's group developed a seed/catalyst-free and selective-growth process for *in situ* growing single-crystalline ZnO NWs on an rGO layer that is abundant with oxygen-containing functional groups.[83] The as-assembled device exhibited a self-driven and fast photoresponse to UV light.

Phototransistor involving QDs/nanoparticles and graphene can offer a unique scheme for high-efficiency exciton dissociation through atomistic design and engineering of the heterojunction.[84,85] This geometry has exhibited distinctive advantages over conventional devices because of not only strong QDs that yield superior electronic and optoelectronic properties such as higher light absorption, charge mobility, and spectra tenability, but also exciton dissociation and charge transfer at the heterojunction interface with favorable interfacial electronic structures for the generation of carriers. Son *et al.* successfully fabricated a highly sensitive colloidal graphene–ZnO QD UV phototransistor using a simple wet spin-coating method. The UV device with ZnO QDs uniformly distributed between the voids of the surface circumferences of the graphene layer displayed a high on/off ratio of 1.1×10^4, and a rise time of 2 s.[86] By systematically analyzing the optoelectronic characteristics of a device with a similar structure,[87] Guo *et al.* observed that the sensitive photoresponse to UV light is largely due to the charge transfer: in the dark, oxygen molecules adsorb on the surface of the QDs and capture free electrons from the n-type ZnO QDs, resulting in a decrease in the conductance of the ZnO QDs. Under UV illumination, photo-generated holes will migrate to the surface and discharge the adsorbed oxygen ions through surface electron–hole recombination [$O_2(ad) + h^+ \rightarrow O_2(g)$], the unpaired electrons thus enhance the conductance.[88] It should be pointed out that the mobility of graphene transistors on SiO_2 is orders of magnitude lower than that of the free-standing graphene, which adversely influences the performance of the above graphene–ZnO QDs phototransistors.[89] In order to improve the carrier mobility of graphene, a feasible method is to insert an organic self-assembled monolayer (SAM) between SiO_2 and graphene as a spacer. As an example, Shao *et al.* demonstrated an ultrasensitive UV phototransistor featuring an organic SAM sandwiched between an inorganic ZnO QD decorated graphene channel and SiO_2 (Fig. 6a–c),[90] in which the electron transit-time in the channel was considerably decreased and the room-temperature mobility of the CVD derived graphene was increased by one order of magnitude (Fig. 6d). The resulting recirculation of the electron increased the photoresponsivity and photoconductive gain of the transistor to $\sim 10^8$ A W^{-1} and $\sim 3 \times 10^9$ (Fig. 6e), respectively, which are comparable to some commercial phototransistors.

To further improve the reproducibility as well as sensitivity of the phototransistors, Gong *et al.* developed a simple precursor printing technology, *via* which a clean van der Waals interface was formed between the ZnO QDs and the graphene layer, enabling high-efficiency exciton dissociation and charge transfer across the graphene–ZnO QD interfaces.[91] This special UV photodetector benefited from the advantages of strong light–mater interaction, quantum confinement of the QDs, and high charge mobility of the graphene. As a result, the device exhibited ultrahigh photoresponsivity up to 9.9×10^8 A W^{-1} and a high detectivity of 7.5×10^{14} Jones. By using a similar precursor

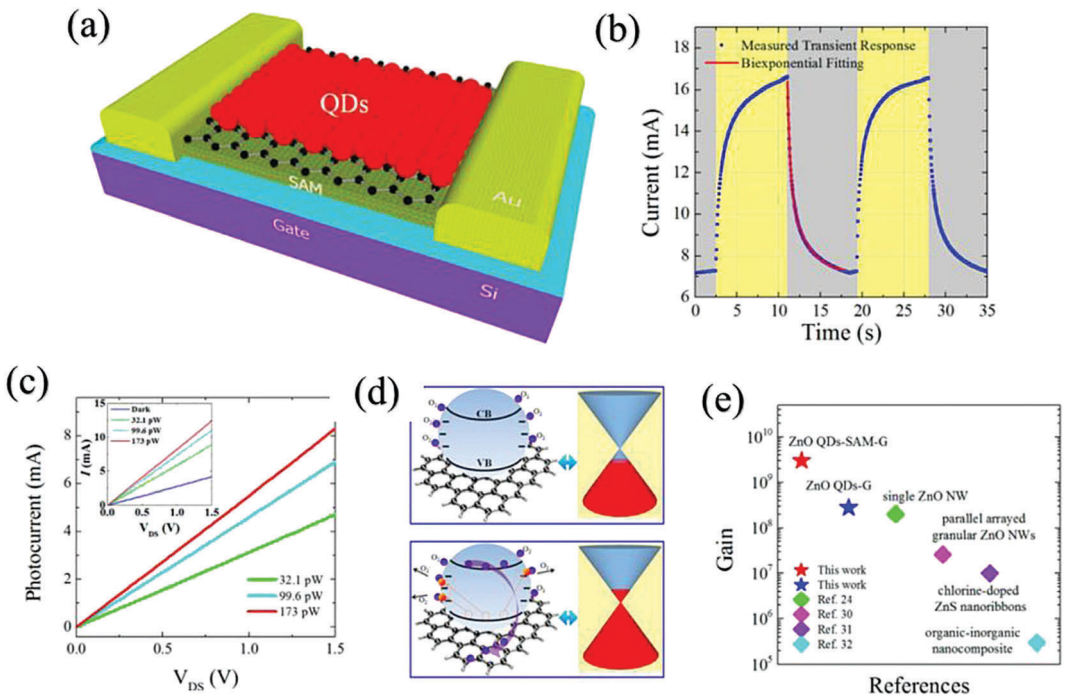

Fig. 6 (a) Device structure of the ultrasensitive graphene–ZnOQD UV phototransistor. (b) Transient response of the UV phototransistor under excitation of 335 nm. (c) Photocurrent of the device under varying light illumination. (d) Schematic illustration of the operation mechanism of the ultrasensitive graphene–ZnOQDs UV phototransistor. (e) Comparison of the photoconductive gain of the present devices and previously reported devices. Reproduced with permission from Shao *et al.*, *Nano Lett.*, 2015, **15**, 3787–3792. Copyright 2015 ACS.

 This journal is © The Royal Society of Chemistry 2018

Published on 19 February 2018. Downloaded by HeFei University of Technology on 20/04/2018 03:48:02.

printing technology, a wafer-size graphene–ZnO nanoparticle UV phototransistor was fabricated.[92] The device achieved a responsivity of 1000 A W^{-1}, and a photoconductive gain of 1.8×10^4. These values are much smaller than that of the printable graphene–ZnO QD device mentioned above, but are at least one order of magnitude higher than that of previously reported UV photodetectors.

3.3 Graphene–ZnO composite UV photodetectors

The last building block for UV sensors is graphene–ZnO composite fiber, which can be fabricated by a simple and one-step electrospinning method across electrodes.[93] During the fabrication process, the duration of operation of electrospinning was vitally important for the alignment of a single nanofiber between prepatterned electrodes. Unlike the conventional ZnO UV sensors that suffer from issues related to the recombination of charge carriers, the UV photodetector assembled from the graphene–ZnO nanocomposite fiber exhibited superior UV sensing with a 1892 fold increase in conductance for 0.5 wt% of graphene. This excellent photoresponse was due to the transfer of photogenerated electrons and holes from ZnO to graphene under UV illumination.

The UV photodetectors composed of rGO–ZnO nanostructure (NPs, NWs or nanofilms) composites have recently attracted huge research interest.[94–96] Taking the rGO–ZnO NPs hybrid structure as an example, Shao and colleagues utilized a simple and one-step chemical method to achieve a ZnO NPs–graphene core–shell structure (Fig. 7a). This geometry was capable of detecting UV illumination with a fast transient response and high responsivity (Fig. 7b and c), which is attributable to the improved structural integrity and carrier transport efficiency through graphene encapsulation (Fig. 7d).[97] In fact, a similar sensitive photoresponse has also been observed on rGO–ZnO NW heterojunctions that were fabricated through separate synthesis of ZnO NWs and graphene, followed by ultrasonic treatment in solution.[98,99] Recently, Wang *et al.* reported a highly sensitive UV photodetector from rGO decorated hydrangea-like ZnO structures on a flexible PDMS substrate.[100] The on/off ratio of the rGO-hydrangea-like ZnO device could be dramatically enhanced upon introduction of an appropriate weight ratio of rGO, and the photocurrent can reach as high as 1 μA and exceed 700 times over that of pure ZnO UV sensors.

4. Graphene–ZnO hybrid structure solar cells

4.1 Dye sensitized solar cells

Dye sensitized solar cells (DSSCs), as a next-generation photovoltaic device, have drawn much interest due to their unique properties and potential applications with low manufacturing cost.[101,102] A typical DSSC consists of a photoanode, sensitizer (dye), electrolyte and counter electrode (CE),[103,104] most of which can be realized by graphene–ZnO hybrid nanostructures.[105–107] Siwach *et al.* reported the application of a

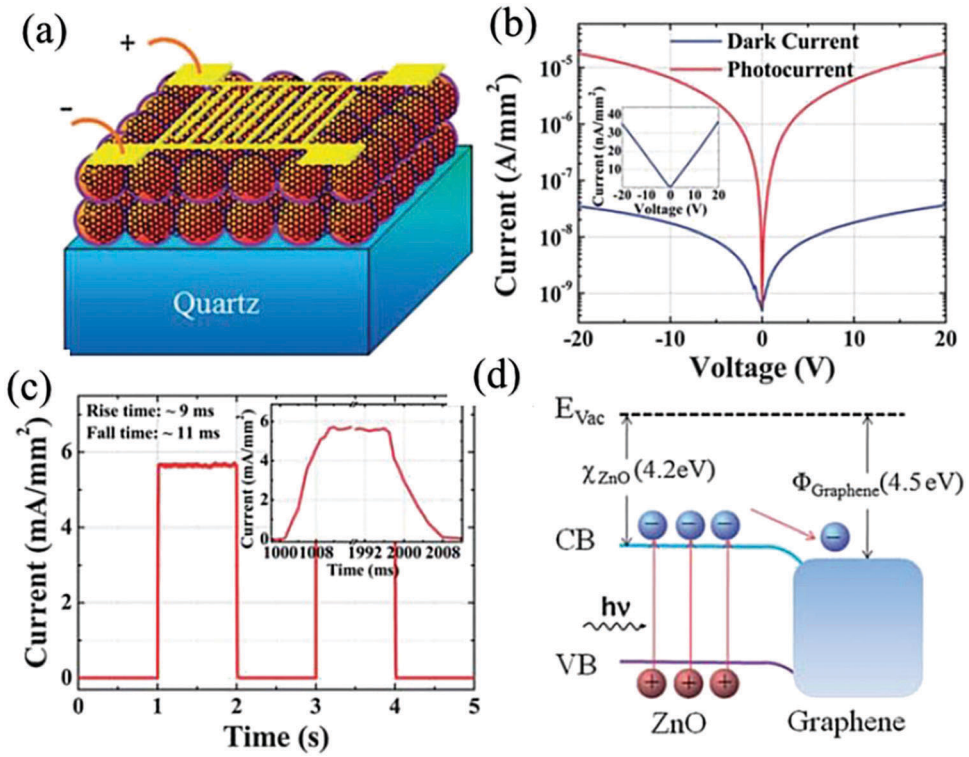

Fig. 7 (a) Schematic of the rGO–ZnO NPs hybrid photodetector. (b) *I–V* characterization of the rGO–ZnO NPs hybrid photodetector. (c) Photoresponse of the rGO–ZnO NPs UV photodetector. (d) Energy band diagram of the rGO–ZnO NPs hybrid photodetector under UV light illumination. Reproduced with permission from Shao *et al.*, *Nanoscale*, 2013, **5**, 3664–3667. Copyright 2013 RSC.

Published on 19 February 2018. Downloaded by HeFei University of Technology on 20/04/2018 03:48:02.

graphene–ZnO composite film for DSSC as a photoanode.[108] A significant increase in short-circuit current (J_{sc}), fill factor (FF), open-circuit voltage (V_{oc}), and power conversion efficiency (PCE) was observed after incorporation of a graphene–ZnO nanocomposite. Understandably, this improvement in device performance is due to the ZnO NPs on the surface of flat graphene, which can make more surface area available for efficient loading of dye molecules on the ZnO NPs.[109,110]

In comparison with ZnO NPs, 1D ZnO nanostructure arrays grown vertically on the substrates can provide a direct electrical pathway to ensure the rapid collection of carriers generated throughout the device and greatly reduce the carrier recombination.[111,112] On this account, vertically aligned ZnO NRs grown on GO–FTO substrates using a low temperature hydrothermal method have been developed as an efficient photoanode for DSSCs, with a PCE of ~2.5%.[113] Such an efficiency is relatively low due to the insufficient surface areas, which limits the absorption of dye and light harvesting efficiency.[114–116] In order to overcome this problem, researchers tried to combine ZnO nanostructures with multidimensional and hierarchical structures. For example, Xu and colleagues modified a ZnO hierarchically structured nanoparticle (HSN) onto 2D graphene scaffolds as the "tentacle" and "speedway", as shown in Fig. 8a.[117] The graphene/ZnO composite photoanode with a highly porous nature is expected to have a higher surface area. It was found that incorporating graphene effectively decreased the internal resistance within the photoanode and prolonged the electron lifetime (Fig. 8b), which can reduce the electron recombination loss and lead to a PCE as high as 3.19% (Fig. 8c).

Another important application of the graphene–ZnO hybrid structure in DSSC is CE. It plays a key role in regulating the DSSC performance by catalyzing the reduction of the iodide–triiodide redox species that are used as a mediator to regenerate the sensitizer after electron injection.[118] A DSSC with a PCE of 0.52% has been fabricated by using graphene–ZnO NPs as CE. The J_{SC} was observed to increase significantly, while the V_{OC} remained nearly unchanged as compared with devices based on ZnO NPs.[119] To reduce the aggregation of graphene, graphene–ZnO NR array hybrid nanostructures have been utilized as CE.[120] Compared to other devices, the graphene–ZnO NRs hybrid DSSC without aggregations had a considerable enhancement in catalytic performance towards the reduction of triiodide, which was confirmed by their electrochemical properties such as high current density, low charge transfer resistance, and narrow peak-to-peak separation. Notably, this graphene–ZnO NR hybrid DSSC had a PCE of 8.12%, with V_{oc}, J_{SC} and FF values of 765 mV, 21.7 mA cm^{-2}, and 67%, respectively, which can nearly compete with that of Pt CE based DSSC.

4.2 Polymer solar cells

Over the past few decades, polymer solar cells (PSCs), have drawn extensive attention due to their potential as renewable,

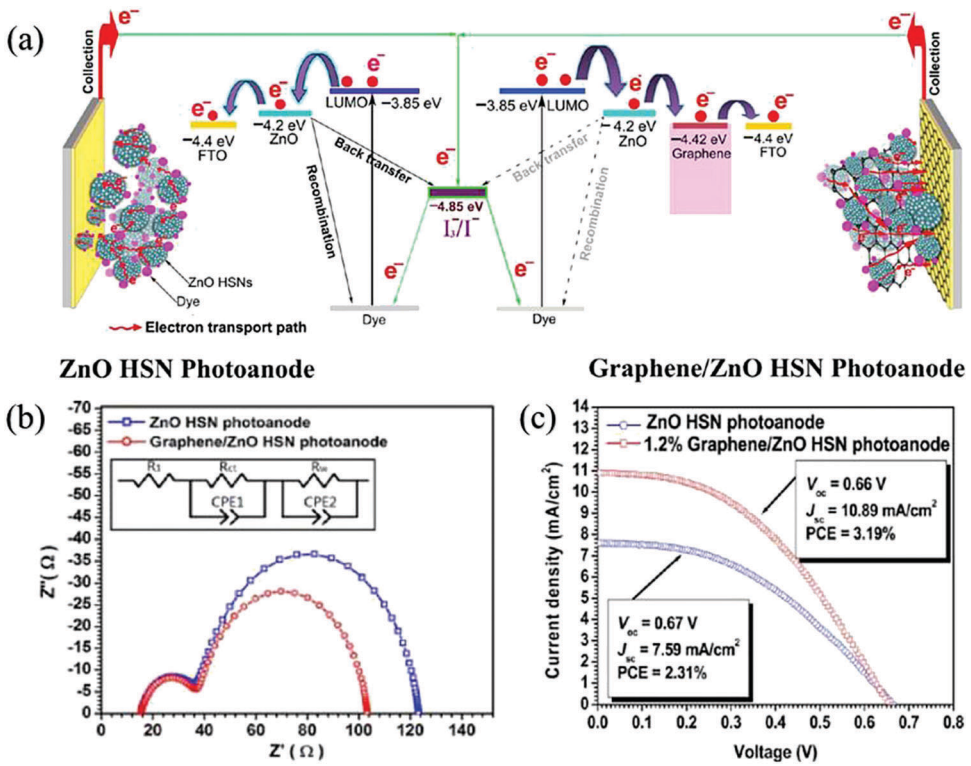

Fig. 8 (a) Schematic illustration of the operation mechanism of the DSSC with ZnO HSN and graphene–ZnO HSN photoanode. (b) Nyquist plots of the electrochemical impedance spectra of the ZnO HSN photoanode and graphene–ZnO HSN photoanode. (c) *J–V* characteristics of the DSSCs assembled using both a ZnO HSN photoanode and graphene–ZnO HSN photoanode. Reproduced with permission from Xu *et al.*, *J. Phys. Chem. C*, 2013, **117**, 8619–8627. Copyright 2013 ACS.

 This journal is © The Royal Society of Chemistry 2018

Published on 19 February 2018. Downloaded by HeFei University of Technology on 20/04/2018 03:48:02.

lightweight, and low-cost energy sources.[121,122] However, it is undeniable that PSCs often suffer from relatively poor air stability, for use of some low work function metal cathodes, such as aluminum and calcium. A possible solution to this issue is to replace these active metals with ZnO nanostructures (*e.g.*, NRs, NPs) or rGO–ZnO nanocomposites.[123–125] Chen's group reported a ZnO@rGO–poly(*N*-vinylpyrrolidone) (PVP) nanocomposite cathode buffer layer by *in situ* growth of ZnO NPs on a rGO–PVP substrate.[126] The PVP not only facilitates the homogenous distribution of the rGO between the PVP and graphene, but also acts as a stabilizer and bridge to direct the growth of ZnO NPs on graphene. Meanwhile, from the perspective of an energy band diagram, the lowest unoccupied molecular orbital (LUMO) level of ZnO was improved once modified with rGO–PVP. As a result, the use of a ZnO@rGO–PVP cathode buffer layer substantially decreases the recombination activity, improves the electrical conductivity, and increases the electron extraction, eventually giving rise to a PCE as high as 7.5% with improved long-term stability. Later on, the same group further increased the PCE to a record value of 8.1% by choosing an amphiphilic fullerene modified 2D graphene–ZnOgraphene–ZnO NRs hybrid as the cathode buffer layer (Fig. 9a).[127] Fig. 9b shows the energy band diagram of ZnO NR arrays, C_{60}–PEG/ZnO NR arrays, ZnO NR arrays@rGO, C_{60}–PEG/ZnO NR arrays@rGO and C_{60}–PEG/ZnO NR arrays@rGO treated by plasma, all of which confirmed a better energy alignment for charge extraction. The fitted curves using the space-charge-limited-current (SCLC) model of electron-only devices are shown in Fig. 9c. Obviously, the electron mobility of the ZnO NR arrays is higher than that of ZnO NPs, and can be further improved by combining with rGO and C_{60}–PEG to as high as 9.56×10^{-4} cm^2 V^{-1} s^{-1}, which could reduce the recombination activity of the carriers.

Like a cathode buffer layer, the electron transport layer (ETL) in PSCs also plays an important part in determining the PCE. To date, while various organic materials and inorganic materials (*e.g.*, TiO_x, and LiF) have been selected as ETL to achieve PSCs with a high PCE, the use of a graphene–ZnO nanocomposite based ETL is also emerging.[128] Hu *et al.* developed an efficient cathode buffer layer by *in situ* growth of ZnO NPs onto a uniformly distributed graphene matrix in ethyl cellulose solution for high performance PSCs.[129] Compared with pure ZnO NPs, the resultant ZnO@graphene:EC possessed higher conductivity, smoother morphology, and lower work function, all of which can facilitate the electron transport and extraction between the active layer and cathode, and reduce the carrier recombination. It was found that the incorporation of a ZnO@graphene:EC nanocomposite as the ETL can lead to a PCE as high as 8.4%.

4.3 Hybrid solar cells

Recently, various bulk heterojunction photovoltaics that integrate a conjugated polymer and inorganic semiconductors have been reported.[130] This unique photovoltaic geometry may take advantage of the beneficial effects of both materials such as the high mobility of inorganic semiconductors and solution processing of

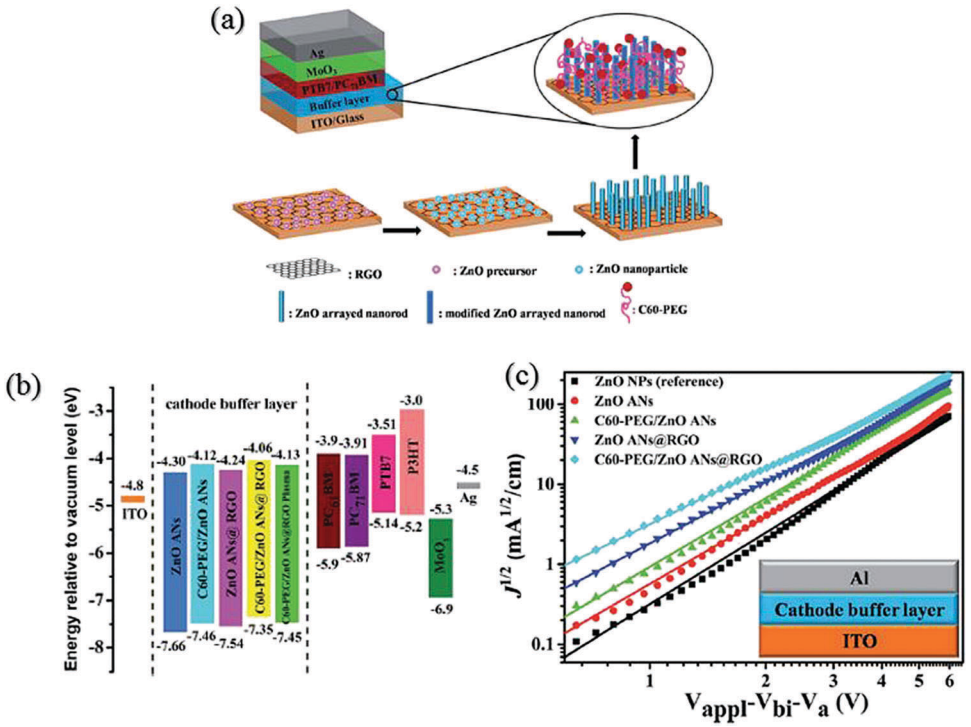

Fig. 9 (a) Schematic illustration of the fabrication process of the C_{60}–PEG modified ZnO NR arrays@rGO cathode buffer layer. (b) The energy level diagram of the ZnO NR arrays, C_{60}–PEG/ZnO NR arrays, ZnO NR arrays@rGO, C_{60}–PEG/ZnO NR arrays@rGO and C_{60}–PEG/ZnO NR arrays@rGO treated by plasma of the devices. (c) Mott–Gurney SCLC fitting log *J*–log *V* plots of the electron-only devices with a structure of ITO/cathode buffer layer/Al, the inset shows the schematic illustration of the electron-only device. Reproduced with permission from Hu *et al.*, *J. Mater. Chem. A*, 2015, **3**, 10890–10899. Copyright 2015 RSC.

Published on 19 February 2018. Downloaded by HeFei University of Technology on 20/04/2018 03:48:02.

organic materials.[131] To optimize the light absorption and carrier transport, various nanocomposites based on graphene/rGO and ZnO nanostructures (*e.g.*, NPs,[132] NWs/NRs,[133] and even nanotubes[134]) have been synthesized to assemble a number of hybrid solar cells with different geometries. Yin *et al.* reported the electrochemical deposition of ZnO NRs on rGO film and utilized the as-synthesized structure to assemble inorganic–organic hybrid solar cells with a layered structure of quartz/rGO/ZnO NRs/P3HT/PEDOT:PSS/Au.[135] Under AM 1.5G illumination, the PCE of the device can reach 0.31%, which is higher than that reported previously. Apart from this study, some hybrid solar cells based on rGO/ZnO/ZnS/poly(3-hexylthiophene) core–shell NR arrays,[136] graphene@ZnONPs:PCPDTBT:PCBM,[137] and graphene-enriched poly(3-hexylthiophene)(G-P3HT) and tetra(4-carboxyphenyle) porphyrin-grafted ZnO NWs arrays have also been developed.[138] These devices exhibited PCEs in the range from 0.4 to 3.65%.

Most hybrid solar cells are assembled on conducting electrodes such as ITO and FTO that have poor contact with the ZnO nanostructure, leading to the accumulation of electrons in the semiconductor layer. Therefore, these devices are often characterized by a relatively low PCE. Graphene with a high electron mobility and outstanding mechanical property becomes a promising candidate as an electrode to replace ITO or FTO in optoelectronic devices. Park *et al.* successfully grew highly uniform ZnO NWs on a graphene sheet by modifying the graphene surface with conductive polymer interlayers (Fig. 10a–c). Using the as-fabricated structure as an ETL, the PCEs can reach 4.2% and 0.5%, respectively, for devices using PbS QDs and P3HT as the photoactive materials (Fig. 10d and e),[139] which are close to ITO-based devices with similar architectures.

4.4 Others

Perovskite solar cells composed of a conducting glass substrate (ITO or FTO), an electron-transporting layer (ETL), an active perovskite layer, a hole-transport layer (HTL) and an electrode, have developed rapidly in the past couples of years,[140,141] owing to the high carrier mobility, direct optical bandgap, broad absorption rang, and low-cost processing of perovskite materials.[142,143] In perovskite solar cells, ZnO/graphene composites have been frequently used as an ETL which is able to transfer electrons from the perovskite layer to the conducting glass substrate. Various studies have shown that the utilization of a ZnO/graphene composite is beneficial for both the PCE and stability in that it can reduce charge recombination, improve charge collection efficiency,[144,145] and prevent decomposition of the perovskite film.[146] Tavakoli and colleagues reported a high performance perovskite solar cell with rGO/ZnO as the ETL. Thanks to the presence of a low amount of hydroxide groups, the perovskite materials exhibited excellent stability on top of

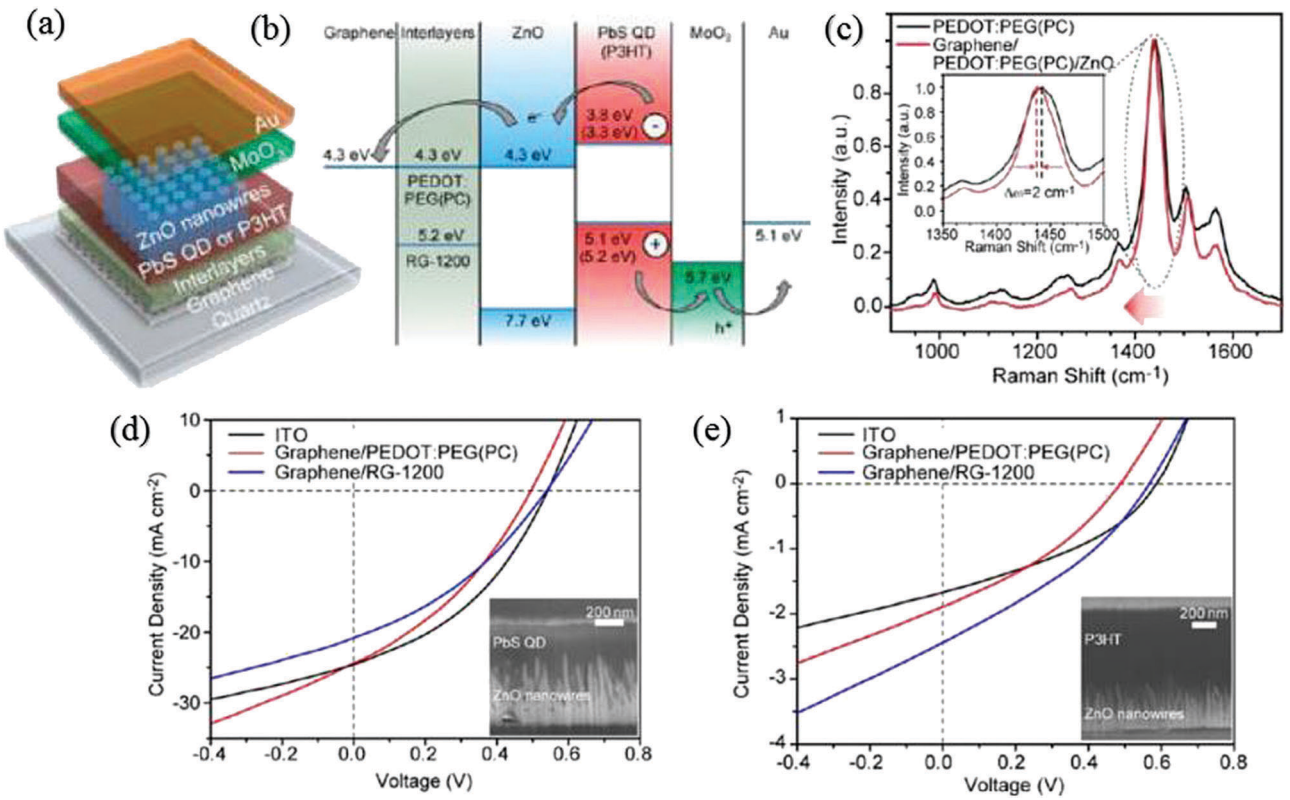

Fig. 10 (a) Schematic illustration of a graphene–ZnO NW based hybrid solar cell. (b) Energy level diagram of the solar cells. (c) Raman peak of the full graphene/PEDOT:PEG(PC)/ZnO hybrid structure solar cell. (d) *J*–*V* characteristics of the champion graphene/ZnO based PbS QDs hybrid solar cells. (e) *J*–*V* characteristics of the champion graphene/ZnO based P3HT hybrid solar cells. Reproduced with permission from Park *et al.*, *Nano Lett.*, 2013, **13**, 233–239. Copyright 2013 ACS.

 This journal is © The Royal Society of Chemistry 2018

Published on 19 February 2018. Downloaded by HeFei University of Technology on 20/04/2018 03:48:02.

the ZnO/rGO layer after annealing at 100 °C. In addition, the rGO/ZnO in the perovskite solar cell could extract the charge carriers quickly from the perovskite layer to reduce the carrier recombination, and thereby increase the EQE and J_{SC} due to a quenching effect. Such a beneficial merit leads to a respectable PCE of 15.2% under AM 1.5G illumination.[147] Recently, graphene/ZnO hybrid structures have also been applied in CdTe and $Cu_2ZnSn(S_xSe_{1-x})_4$ (CZTSSe) based solar cells.[148] The PCE of the hybrid structure based solar cells is close to that of ITO-based devices with similar architectures, suggesting that the graphene–ZnO heterostructure is a potential alternative for ITO in solar cells.[149]

5. Graphene–ZnO hybrid structure LEDs

By virtue of the unavailability of high-quality and stable p-type ZnO materials,[150,151] the development of ZnO-based homojunction light emitting devices has been a great challenge.[152,153] An alternative way to achieve ZnO-based UV electroluminescence (EL) is to fabricate heterojunction LEDs by utilizing other available p-type materials (*e.g.*, p-GaN, p-Si, p-NiO, and p-type organic materials). Chung *et al.* reported a hetero-epitaxial method to grow high-quality GaN on ZnO thin film-coated graphene layers and transferred it onto arbitrary substrates (Fig. 11a).[154] To fabricate LED, n-GaN, $In_xGa_{1-x}N$/GaN multiple-quantum-well (MQW) were deposited on the GaN film grown on graphene layers, as shown in Fig. 11b. A potential advantage is that lattice mismatch may not be considered seriously because the graphene layers have weak bonding to each other. Power-dependent EL spectra of the LED and optical images of the emissions at room temperature showed an increase of emission intensity with the applied current levels of 5.1, 6.4, and 8.1 mA (Fig. 11c and d). This group later on successfully developed high-quality and flexible GaN/ZnO coaxial NRs heterostructures LEDs by directly growing a high-quality GaN p–n homojunction on a graphene–ZnO NR array.[155] The LEDs with strong blue emission were readily transferred onto flexible plastic substrates, which operate reliably in a flexible form without

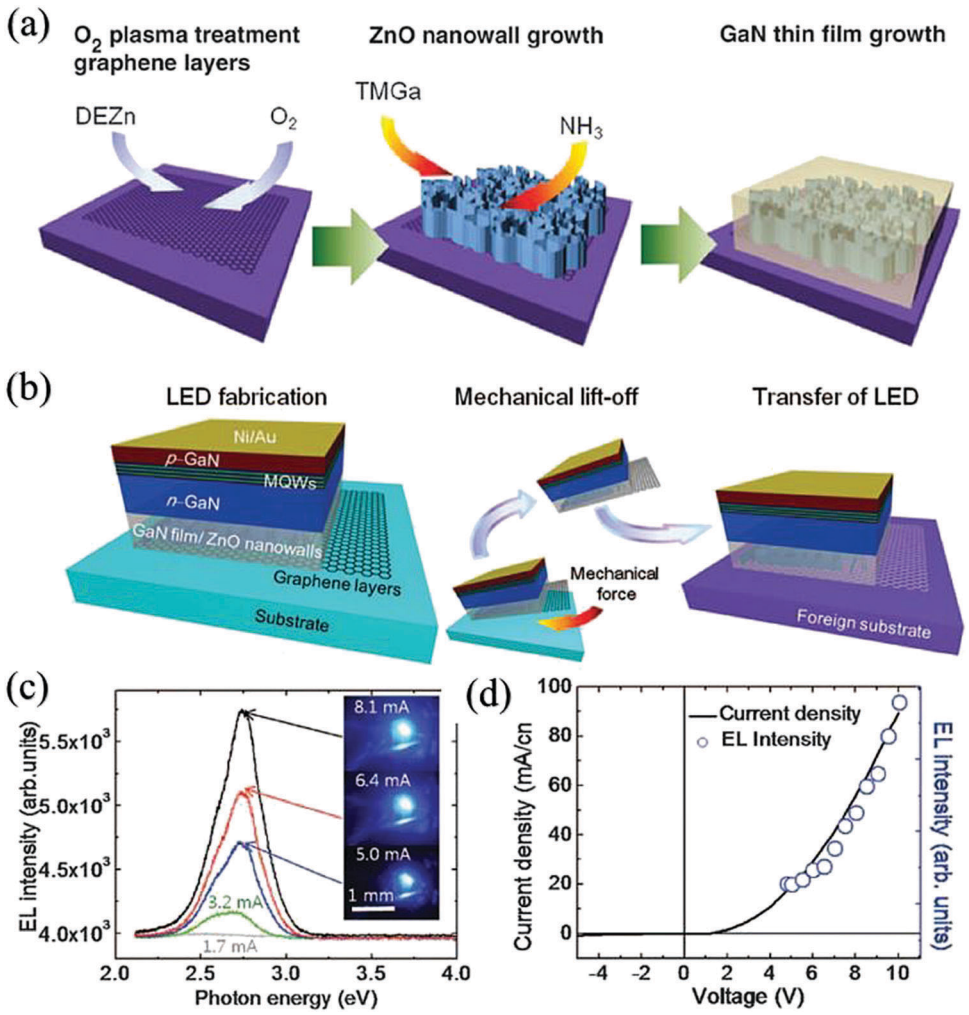

Fig. 11 (a) The fabrication processes for epitaxial GaN thin films. (b) Schematic illustration of the fabrication and transfer processes for thin-film LEDs. (c) EL spectra of the LED transferred onto a plastic substrate, the inset shows the light emission at different applied current levels of 1.7–8.0 mA. (d) Current density and integrated EL intensity as a function of the applied bias voltage of a representative LED on a plastic substrate. Reproduced with permission from Chung *et al.*, *Science*, 2010, **330**, 655–657. Copyright 2010 AAAS.

Published on 19 February 2018. Downloaded by HeFei University of Technology on 20/04/2018 03:48:02.

obvious degradation in performance. Moreover, some similar LED devices based on graphene/ZnO NR/p-GaN,[156,157] graphene/ZnO NRs/GaN/InGaN,[158] and rGO/ZnO:Ga NR/GaN were reported as well. These devices exhibited an improved EL performance when compared with other conventional structures using ITO as the current spreading layer.[159] In addition to epitaxial substrate or current spreading current, graphene–ZnO NRs array hybrid structures have also been incorporated into GaN as a transparent conductive layer for low work voltage and high light extraction.[160]

In spite of the wide use of hybrid structures combining ZnO nanomaterials and graphene sheets in various LEDs, the absence of bandgap in graphene has greatly restricted the emissive properties. A reliable solution to this issue is to use emissive ZnO QDs or GQDs, which can emit light with an adjustable wavelength. Son *et al.* reported the synthesis of emissive hybrid QDs composed of a ZnO QD core wrapped in a shell of monolayer graphene for white LED with a brightness of 798 cd m^{-2}.[161] New blue emissions were found from the graphene–ZnO QDs, which can be correlated with an electronic transition from LUMO and LUMO+2 to the ZnO valence band. White LED can also be achieved by synthesizing CdTe/ZnO/rGO quasi–core–shell–shell hybrid colloidal QDs (Fig. 12a), with a unique PL peak at 624 nm related to the CdTe core and additional peaks at 382, 404, 422, 440 nm attributable to the ZnO/rGO composite (Fig. 12b).[162] As shown in Fig. 12c, multiple emission peaks are observed in the EL spectrum, which can be correlated to the recombination of carriers from LUMO and LUMO+2 of GO and holes in the valence band (V_B) of ZnO and recombination process inside the CdTe core. Overall, the QD LED showed clear white color emission with a maximum luminance value of about 480 cd m^{-2} with CIE coordinates (0.35, 0.28). Additionally, a hybrid structure consisting of ZnO and graphene QD has been widely used in some flexible polymer LEDs that exhibited improved device stability,[163] or higher current densities.[164]

6. Graphene–ZnO hybrid structure lasers

A laser is an optoelectronic device that converts energy into light with a mechanism for emitting electromagnetic radiation *via* stimulated emission.[165] Hitherto, UV lasing of ZnO has been observed in various micro/nanostructures through random[166] Fabry–Perot (F–P)[167] and whispering-gallery mode (WGM)[168] resonant approaches. Nevertheless, due to huge cavity losses and the diffraction limit,[169] it is challenging to realize a high lasing output or miniaturized dimension lasers with high efficiency. Surface plasmon (SP)-mediated PL enhancement has already been observed at metal or metal alloy/ZnO interfaces,[170] yet with difficulties of flexible design and development of novel functional photonic materials and devices, owing to a lack of flexibility in rigid devices and the large Ohmic losses.[171,172] Various recent studies have shown that graphene has a very high quantum efficiency for light–matter interaction and strong

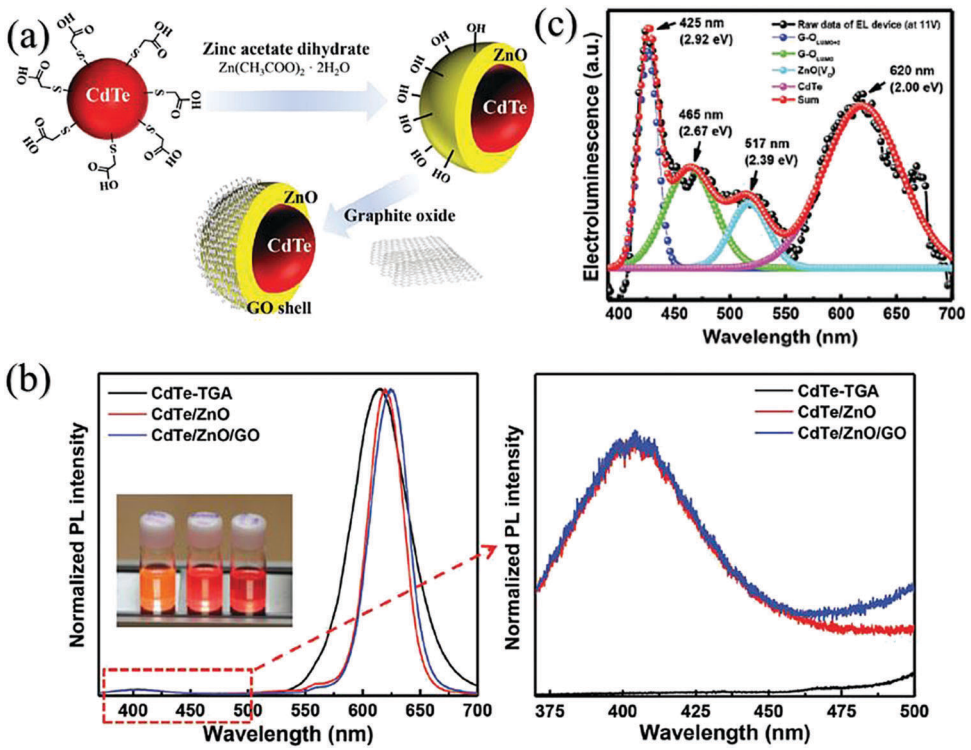

Fig. 12 (a) Schematic illustration of the chemical synthesis process of CdTe/ZnO/rGO quasi–core–shell–shell QDs. (b) Normalized PL spectra obtained from CdTe–TGA, CdTe/ZnO and CdTe/ZnO/rGO. (c) EL spectra of white LED. Reproduced with permission from Kim *et al.*, *Nanoscale*, 2016, **8**, 19737–19743. Copyright 2016 RSC.

 This journal is © The Royal Society of Chemistry 2018

Published on 19 February 2018. Downloaded by HeFei University of Technology on 20/04/2018 03:48:02.

plasmons, rendering graphene/ZnO as an ideal candidate for UV lasing.[173] Li *et al.* reported on the induction of optical field confinement by graphene SP in a graphene-coated ZnO microrod, which acted as a whispering-gallery microcavity for lasing resonance.[174] The district optical confinement and PL enhancement were experimentally observed, consistent with the theoretical simulations. As a functional application, improved WGM lasing performance with stronger lasing intensity, lower threshold, and a high-quality (Q) factor was realized. Through the coupling between graphene SP modes and optical microcavity modes of ZnO microbelt, enhanced F–P lasing performance was realized as well, including alowered lasing threshold, improved lasing quality and remarkably enhanced lasing intensity.[175]

High performance single-mode lasing has attracted intensive interest due to its high Q factor, lasing threshold and narrow spectral line width based on the total internal-wall reflection of the microcavity.[176] Xu's group realized single-mode lasing resonance in a sub-micro ZnO rod based on serially varying the dimension of the WGM cavities (Fig. 13a and b).[177] The lasing quality factor and lasing intensity were substantially increased by covering single layer graphene on the ZnO submicron-rod. Graphene-induced optical field confinement and lasing emission enhancement were revealed, indicative of an energy coupling between graphene SP and ZnO exciton emission (Fig. 13c–e). Raman scatting processes can convert pump lasers into new frequencies. The development of a Raman laser may allow tunable nanolasers and boost the development of innovative nanophotonics technology. Ruan's group reported the growth of a ZnO–graphene superlattice *via* a spatially confined reaction method for room-temperature thresholdless tunable Raman lasing. This Raman nanolaser is tunable from the visible to NIR range. A new mechanism called "selective surface plasmon amplification by stimulated Raman scattering" was believed to be responsible for the generation of the Raman nanolaser.[178]

7. Conclusion and outlook

Graphene–ZnO hybrid heterostructures have proved to be promising building blocks for assembling high-performance optoelectronic devices that can overcome intrinsic limitations of graphene. In this paper, we present a comprehensive survey of recent achievements in the development of graphene–ZnO hybrid heterostructures for various optoelectronic device applications, such as photodetectors, solar cells, LEDs and lasers. We start by introducing the synthetic methodology of either bottom-up or top-down methods, followed by device performance analysis of different optoelectronic devices. Particular attention has been given to some critical issues that pertain to the device design, device performance and physics, and the processing techniques for performance optimization.

Even though graphene–ZnO hybrid heterojunction based optoelectronic devices have been around for less than 10 years, there are some great breakthroughs that deserve special attention. To name a few, the responsivity of the first graphene–ZnO hybrid UV light photodetector was only 0.5 A W^{-1} in 2012, and was recently improved to 9.9×10^8 A W^{-1}. What is more, the detectivity was improved from 3.9×10^{13} to 7.5×10^{14} Jones, which can nearly compete with commercial Si-based photodetectors. Similar progresses have also been made in graphene–ZnO based solar cells.

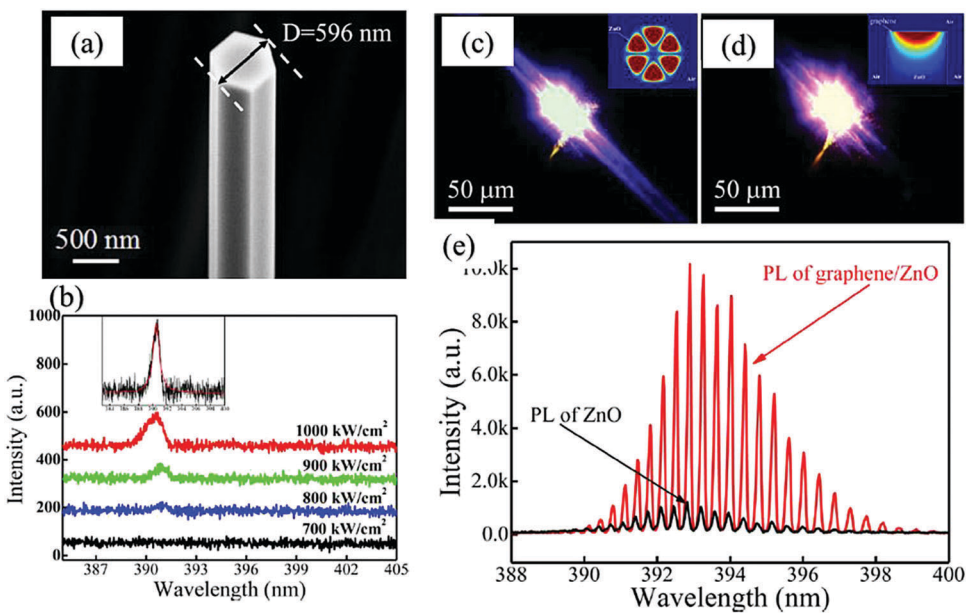

Fig. 13 (a) SEM image of one submicron-sized ZnO rod with a diameter of 596 nm and a smooth side surface. (b) The PL spectra of a bare submicron-sized ZnO rod and (f) the same ZnO covered with graphene under different excitation power densities. Dark field optical images of an individual ZnO microrod (c) before and (d) after being covered with graphene under the same excitation conditions. (e) Comparison of the PL spectra from the same ZnO microrod before (black line) and after (red line) graphene covering. Reproduced with permission from Li *et al.*, *ACS Nano*, 2015, **9**, 6794–6800. Copyright 2015 ACS.

Published on 19 February 2018. Downloaded by HeFei University of Technology on 20/04/2018 03:48:02.

The first solar cell that used graphene–ZnO NPs as the CE had a PCE of only 0.52% in 2013. By reducing the aggregation of graphene with a graphene–ZnO NR array hybrid nanostructure, the PCE was substantially improved to 8.12%, which can nearly compete with that of Pt CE based DSSC.

In spite of the above achievements, there are still some unresolved issues. For photodetectors, there is much space to improve the responsivity, sensitivity and response speed. For example, it is feasible to optimize the properties of some sensing materials, *e.g.*, more precise control of their morphology, hierarchical, crystallinity, orientation assembly, as well as physical and chemical properties such as carrier transport characteristics. Also, novel device designs including plasmonic techniques and integration with microcavities are useful avenues to enhance light–matter interaction for optical absorption enhancement. In addition, the uniformity of the sensing materials should be taken into consideration and the integration of photodetectors should be further explored to facilitate commercial applications. For solar cells, the PCE is still much lower in comparison to that of commercial Si-based solar cells. Therefore, to further improve the efficiency, particular attention should be given to optimizing the properties of the materials and rational device design. For instance, the sheet conductivity and work function of graphene can be optimized to facilitate more efficient transport and collection of photocarriers. Some passivation and modification schemes are also useful to optimize the band alignment and reduce charge carrier recombination. In addition, introducing new optoelectronic materials and structures may offer opportunities to further improve the device performance. Furthermore, due to excellent mechanical strength and elasticity of graphene, ZnO–graphene could be transferred to foreign substrates to extend their application in flexible and wearable optoelectronics. To realize practical applications, besides the performance improvement, long-term stability and durability, environment-friendly and cost-effective processing, as well as large-scale production and integration are some of the most important issues that need to be tackled in future research. In light of the simple device architecture, low-cost manufacturing process and the relatively high device performance, the ZnO/graphene hybrid heterostructures will provide a prospective platform for the development of high-performance optoelectronic devices in the future.

Conflicts of interest

There are no conflicts to declare.

Acknowledgements

This work was supported by the National Natural Science Foundation of China (NSFC, No. 61575059, 61675062, 21501038), the Fundamental Research Funds for the Central Universities (JZ2015HGXJ0184, JZ2016HGBZ1046), the Anhui Natural Science Foundation of China (No. 1708085ME122), and the China Postdoctoral Science Foundation (103471013).

References

1 S. Baskoutas and G. Bester, *J. Phys. Chem. C*, 2011, **115**, 15862.
2 E. Comini, G. Faglia, G. Sberveglieri, Z. W. Pan and Z. L. Wang, *Appl. Phys. Lett.*, 2002, **81**, 1869.
3 Z. L. Wang, *Mater. Today*, 2004, **7**, 26.
4 E. Fortunato, P. Barquinha and R. Martins, *Adv. Mater.*, 2012, **24**(22), 2945.
5 X. D. Wang, J. Zhou, J. H. Song, N. S. Xu and Z. L. Wang, *Nano Lett.*, 2006, **6**, 2768.
6 Y. Zhang, J. Q. Xu, Q. Xiang, Q. Y. Pan and P. C. Xu, *J. Phys. Chem. C*, 2009, **113**, 3430.
7 Q. Wan, Q. H. Li, Y. J. Chen, T. H. Wang, X. L. He, J. P. Li and C. L. Lin, *Appl. Phys. Lett.*, 2004, **84**, 3654.
8 W. Y. Chang, Y. C. Lai, T. B. Wu, S. F. Wang, F. Chen and M. J. Tsai, *Appl. Phys. Lett.*, 2008, **92**, 022110.
9 Z. L. Wang and J. H. Song, *Science*, 2006, **312**, 242.
10 X. Y. Kong and Z. L. Wang, *Nano Lett.*, 2003, **3**, 1625.
11 Q. F. Zhang, C. S. Dandeneau, X. Y. Zhou and G. Z. Cao, *Adv. Mater.*, 2009, **21**, 4087.
12 A. B. F. Martinson, J. W. Elam, J. T. Hupp and M. J. Pellin, *Nano Lett.*, 2007, **7**, 2183.
13 J. M. Bao, M. A. Zimmler, F. Capasso, X. W. Wang and Z. F. Ren, *Nano Lett.*, 2006, **6**, 1719.
14 X. B. Tang, G. M. Li and S. M. Zhou, *Nano Lett.*, 2013, **13**, 5046–5050.
15 C. Soci, A. Zhang, B. Xiang, S. A. Dayeh, D. P. R. Aplin, J. Park, X. Y. Bao, Y. H. Lo and D. Wang, *Nano Lett.*, 2007, **7**, 1003.
16 M. H. Huang, S. Mao, H. Feick, H. Yan, Y. Wu, H. Kind, E. Weber, R. Russo and P. D. Yang, *Science*, 2001, **292**, 1897.
17 D. C. Wei and Y. Q. Liu, *Adv. Mater.*, 2010, **22**, 3225.
18 K. S. Novoselov, A. K. Geim, S. V. Morozov, D. Jiang, Y. Zhang, S. V. Dubonos, I. V. Grigorieva and A. A. Firsov, *Science*, 2004, **306**, 666.
19 K. S. Novoselov, A. K. Geim, S. V. Morozov, D. Jiang, M. I. Katsnelson, I. V. Grigorieva, S. V. Dubonos and A. A. Firsov, *Nature*, 2005, **438**, 197.
20 F. H. L. Koppens, T. Mueller, P. Avouris, A. C. Ferrari, M. S. Vitiello and M. Polini, *Nat. Nanotechnol.*, 2014, **9**, 780.
21 Q. L. Bao and K. P. Loh, *ACS Nano*, 2012, **6**, 3677.
22 A. M. Munshi, D. L. Dheeraj, V. T. Fauske, D. C. Kim, A. T. J. van Helvoort, B. O. Fimland and H. Weman, *Nano Lett.*, 2012, **12**, 4570.
23 J. M. Lee, Y. B. Pyun, J. Yi, J. W. Choung and W. I. Park, *J. Phys. Chem. C*, 2009, **113**, 19134.
24 K. Ul Hasan, M. O. Sandberg, O. Nur and M. Willander, *Adv. Opt. Mater.*, 2014, **2**, 326.
25 C. Xie, C. Mak, X. Tao and F. Yan, *Adv. Funct. Mater.*, 2017, **27**, 1603886.
26 W. Bao, L. Jing, J. Velasco, Y. Lee, G. Liu, D. Tran, B. Standley, M. Aykol, S. B. Cronin, D. Smirnov, M. Koshino, E. McCann, M. Bockrath and C. N. Lau, *Nat. Phys.*, 2011, **7**, 948.
27 M. L. Lu, H. Y. Lin, T. T. Chen and Y. F. Chen, *Appl. Phys. Lett.*, 2011, **99**, 091106.
28 J. M. Lee, J. Yi, W. W. Lee, H. Y. Jeong, T. Jung, Y. Kim and W. I. Park, *Appl. Phys. Lett.*, 2012, **100**, 061107.

 This journal is © The Royal Society of Chemistry 2018

Published on 19 February 2018. Downloaded by HeFei University of Technology on 20/04/2018 03:48:02.

29 S. Kim, D. B. Janes, S. Y. Choi and S. Ju, *Appl. Phys. Lett.*, 2012, **101**, 063122.
30 H. Zhang, A. V. Babichev, G. Jacopin, P. Lavenus, F. H. Julien, A. Yu. Egorov, J. Zhang, T. Pauporté and M. Tchernycheva, *J. Appl. Phys.*, 2013, **114**, 234505.
31 W. Yang and X. Hu, *Phys. Rev. Lett.*, 2011, **107**, 127403.
32 B. G. Chen, C. Meng, Z. Y. Yang, W. Li, S. S. Lin, T. Y. Gu, X. Guo, D. L. Wang, S. L. Yu, C. W. Wong and L. M. Tong, *Opt. Express*, 2014, **22**, 24276.
33 B. Nie, J. G. Hu, L. B. Luo, C. Xie, L. H. Zeng, P. Lv, F. Z. Li, J. S. Jie, M. Feng, C. Y. Wu, Y. Q. Yu and S. H. Yu, *Small*, 2013, **9**, 2872.
34 W. Y. Kong, G. A. Wu, K. Y. Wang, T. F. Zhang, Y. Y. Wang, D. D. Wang and L. B. Luo, *Adv. Mater.*, 2016, **28**, 10725.
35 M. Z. Wang, F. X. Liang, B. Nie, L. H. Zeng, L. X. Zheng, P. Lv, Y. Q. Yu, C. Xie, Y. Y. Li and L. B. Luo, *Part. Part. Syst. Charact.*, 2013, **30**, 630.
36 L. B. Luo, C. Xie, X. H. Wang, Y. Q. Yu, C. Y. Wu, H. Hu, K. Y. Zhou, X. W. Zhang and J. S. Jie, *Nano Energy*, 2014, **9**, 112.
37 Y. J. Kim, Hadiyawarman, A. Yoon, M. Kim, G. C. Yi and C. L. Liu, *Nanotechnology*, 2011, **22**, 245603.
38 H. Liu, Q. Sun, J. Xing, Z. Y. Zheng, Z. L. Zhang, Z. Q. Lu and K. Zhao, *ACS Appl. Mater. Interfaces*, 2015, **7**, 6645.
39 J. L. Wu, X. P. Shen, L. Jiang, K. Wang and K. M. Chen, *Appl. Surf. Sci.*, 2010, **256**, 2826.
40 B. Saravanakumar, R. Mohan and S. J. Kim, *Mater. Res. Bull.*, 2013, **48**, 878.
41 N. S. A. Aziz, M. R. Mahmood, K. Yasui and A. M. Hashim, *Nanoscale Res. Lett.*, 2014, **9**, 95.
42 N. S. A. Aziz, T. Nishiyama, N. I. Rusli, M. R. Mahmood, K. Yasui and A. M. Hashim, *Nanoscale Res. Lett.*, 2014, **9**, 337.
43 C. J. Xu, B. S. Kim, J. H. Lee, M. J. Kim, S. W. Hwang, B. L. Choi, E. K. Lee, J. M. Kim and D. M. Whang, *Mater. Lett.*, 2012, **72**, 25.
44 A. Ali, K. Ali, Y. J. Yang, J. Jo and K. H. Choi, *Jpn. J. Appl. Phys.*, 2014, **53**, 05HA01.
45 Y. Zeng, Y. Zhao and Y. J. Jiang, *Appl. Surf. Sci.*, 2014, **301**, 391.
46 J. Lin, M. Penchev, G. P. Wang, R. K. Paul, J. B. Zhong, X. Y. Jing, M. Ozkan and C. S. Ozkan, *Small*, 2010, **6**, 2448.
47 S. H. Cheng, Y. C. Yeh, M. L. Lu, C. W. Chen and Y. F. Chen, *Opt. Express*, 2012, **20**, 799.
48 L. B. Luo, X. B. Yang, F. X. Liang, J. S. Jie, Q. Li, Z. F. Zhu, C. Y. Wu, Y. Q. Yu and L. Wang, *CrystEngComm*, 2012, **14**, 1942.
49 Y. J. Kim, J. H. Lee and G. C. Yi, *Appl. Phys. Lett.*, 2009, **95**, 213101.
50 A. F. Kohan, G. Ceder, D. Morgan and C. G. Van de Walle, *Phys. Rev. B: Condens. Matter Mater. Phys.*, 2000, **61**, 15019.
51 A. Janotti and C. G. Van de Walle, *Phys. Rev. B: Condens. Matter Mater. Phys.*, 2007, **76**, 165202.
52 H. B. Zeng, G. T. Duan, Y. Li, S. K. Yang, X. X. Xu and W. P. Cai, *Adv. Funct. Mater.*, 2010, **20**, 561.
53 L. Schmidt-Mende and J. L. Macmanus-Driscoll, *Mater. Today*, 2007, **10**, 40.
54 M. D. McCluskey and S. J. Jokela, *J. Appl. Phys.*, 2009, **106**, 071101.
55 C. Soci, A. B. Xiang, S. A. Dayeh, D. P. R. Aplin, J. Park, X. Y. Bao, Y. H. Lo and D. Wang, *Nano Lett.*, 2007, **7**, 1003.
56 X. Y. Xu, C. X. Xu and J. G. Hu, *J. Appl. Phys.*, 2014, **116**, 103105.
57 Z. Zhang, Q. L. Liao, Y. H. Yu, X. D. Yu and Y. Zhang, *Nano Energy*, 2014, **9**, 237.
58 C. C. Cheng, J. Y. Zhan, Y. M. Liao, T. Y. Lin, Y. P. Hsieh and Y. F. Chen, *Appl. Phys. Lett.*, 2016, **109**, 053501.
59 H. Y. Yang, D. I. Son, T. W. Kim, J. M. Lee and W. Park, *Org. Electron.*, 2010, **11**, 1313.
60 H. Lee, N. An, S. Jeong, S. H. Kang, S. Kwon, J. Lee, Y. Lee, D. Y. Kim and S. Lee, *Curr. Appl. Phys.*, 2017, **17**, 552.
61 D. L. Shao, X. Sun, M. Xie, H. T. Sun, F. Y. Lu, S. M. George, J. Lian and S. Sawyer, *Mater. Lett.*, 2013, **112**, 165.
62 T. F. Zhang, G. A. Wu, J. Z. Wang, Y. Q. Yu, D. Y. Zhang, D. D. Wang, J. B. Jiang, J. M. Wang and L. B. Luo, *Nanophotonics*, 2017, **6**, 1073.
63 L. Duan, F. N. He, Y. Tian, B. Sun, J. B. Fan, X. C. Yu, L. Ni, Y. Zhang, Y. N. Chen and W. X. Zhang, *ACS Appl. Mater. Interfaces*, 2017, **9**, 8161.
64 J. W. Liu, R. T. Lu, G. W. Xu, J. Wu, P. Thapa and D. Moore, *Adv. Funct. Mater.*, 2013, **23**, 4941.
65 X. W. Fu, Z. M. Liao, Y. B. Zhou, H. C. Wu, Y. Q. Bie, J. Xu and D. P. Yu, *Appl. Phys. Lett.*, 2012, **100**, 223114.
66 B. D. Boruah, A. Mukherjee and A. Misra, *Nanotechnology*, 2016, **27**, 095205.
67 B. D. Boruah, D. B. Ferry, A. Mukherjee and A. Misra, *Nanotechnology*, 2015, **26**, 235703.
68 A. M. Bazargan, F. Sharif, S. Mazinani and N. Naderi, *J. Mater. Sci.: Mater. Electron.*, 2017, **28**, 11108.
69 H. Liu, Q. Sun, J. Xing, Z. Y. Zheng, Z. Zhang, Z. Q. Lv and K. Zhao, *ACS Appl. Mater. Interfaces*, 2015, **7**, 6645.
70 S. Dhar, T. Majumder and S. P. Mondal, *ACS Appl. Mater. Interfaces*, 2016, **8**, 31822.
71 R. Liu, X. C. You, X. W. Fu, F. Lin, J. Meng, D. P. Yu and Z. M. Liao, *Sci. Rep.*, 2015, **5**, 10125.
72 S. Lee, Y. Lee, D. Y. Kim, E. B. Song and S. M. Kim, *Appl. Phys. Lett.*, 2013, **102**, 041301.
73 P. Sahatiya, S. S. Jones, T. Gomathi and S. Badhulika, *2D Mater.*, 2017, **4**, 025053.
74 S. Liu, Q. L. Liao, S. N. Lu, Z. Zhang, G. J. Zhang and Y. Zhang, *Adv. Funct. Mater.*, 2016, **26**, 1347.
75 Z. Wu, X. Li, H. Zhong, S. Zhang, P. Wang, T. H. Kim, S. S. Kwak, C. Liu, H. S. Chen, S. W. Kim and S. S. Lin, *Opt. Express*, 2015, **23**, 18864.
76 Q. Xu, Q. J. Cheng, J. X. Zhong, W. W. Cai, Z. F. Zhang, Z. Y. Wu and F. Y. Zhang, *Nanotechnology*, 2014, **25**, 055501.
77 G. Konstantatos, M. Badioli, L. Gaudreau, J. Osmond, M. Bernechea, F. P. Carcia de Arquer, F. Gatti and F. H. L. Koppens, *Nat. Nanotechnol.*, 2012, **7**, 363.
78 M. Kumar, Y. Noh, K. Polat, A. K. Okyay and D. Lee, *Solid State Commun.*, 2015, **224**, 37.
79 V. Q. Dang, T. Q. Trung, D. I. Kim, L. T. Duy, B. U. Hwang, D. W. Lee, B. Y. Kim, L. D. Toan and N. E. Lee, *Small*, 2015, **25**, 2053.

Published on 19 February 2018. Downloaded by HeFei University of Technology on 20/04/2018 03:48:02.

80 V. Q. Dang, T. Q. Trung, L. T. Duy, B. Y. Kim, S. Siddiqui, W. Lee and N. E. Lee, *ACS Appl. Mater. Interfaces*, 2015, **7**, 11032.
81 B. D. Boruah, A. Mukherjee, S. Srishar and A. Misra, *ACS Appl. Mater. Interfaces*, 2015, **7**, 10606.
82 R. K. Biroju, N. Tilak, G. Rajender, S. Dhara and P. K. Giri, *Nanotechnology*, 2015, **26**, 145601.
83 H. Yang, J. L. Li, D. C. Yu and L. Li, *Cryst. Growth Des.*, 2016, **16**, 4831.
84 B. D. Boruah and A. Misra, *RSC Adv.*, 2015, **5**, 90838.
85 Z. Y. Zhan, L. X. Zheng, Y. Z. Pan, G. Z. Sun and L. Li, *J. Mater. Chem.*, 2012, **22**, 2589.
86 D. I. Son, H. Y. Yang, T. W. Kim and W. Park, *Appl. Phys. Lett.*, 2013, **102**, 021105.
87 D. I. Son, H. Y. Yang, T. W. Kim and W. Park, *Composites, Part B*, 2015, **69**, 154.
88 W. H. Guo, S. G. Xu, Z. F. Wu, N. Wang, M. M. T. Loy and S. W. Du, *Small*, 2013, **9**, 3031.
89 J. H. Chen, C. Jang, S. Adam, M. S. Fuhrer, E. D. Williams and M. Ishigami, *Nat. Phys.*, 2007, **4**, 377.
90 D. L. Shao, J. Gao, P. Chow, H. T. Sun, G. Q. Xin, P. Sharma, J. Lian, N. A. Koratkar and S. Sawyer, *Nano Lett.*, 2015, **15**, 3787.
91 M. G. Gong, Q. F. Liu, B. Cook, B. Kattel, T. Wang, W. L. Chan, D. Ewing, M. Casper, A. Stramel and J. Z. Wu, *ACS Nano*, 2017, **11**, 4114.
92 Q. F. Liu, M. G. Gong, B. Cook, D. Ewing, M. Casper, A. Stramel and J. Wu, *J. Mater. Chem. C*, 2017, **5**, 6427.
93 P. Sahatiya and S. Badhulika, *RSC Adv.*, 2015, **5**, 82481.
94 A. N. Fouda, A. B. El Basaty and E. A. Eid, *Nanoscale Res. Lett.*, 2016, **11**, 13.
95 S. Darbari, V. Ahmadi, P. Afzali, Y. Abdi and M. Feda, *J. Nanopart. Res.*, 2014, **16**, 2798.
96 H. X. Chang, Z. H. Sun, K. Y. Ho, X. M. Tao, F. Yan, W. M. Kwok and Z. J. Zheng, *Nanoscale*, 2011, **3**, 258.
97 D. L. Shao, M. P. Yu, H. T. Sun, T. Hu, J. Lian and S. Sawyer, *Nanoscale*, 2013, **5**, 3664–3667.
98 X. B. Liu, H. J. Du and X. W. Sun, *RSC Adv.*, 2014, **4**, 5136.
99 X. L. Ye, H. Liu, N. T. Hu, J. Wang, M. Li and Y. F. Zhang, *Mater. Lett.*, 2015, **150**, 126.
100 Z. X. Wang, X. Y. Zhan, Y. J. Wang, S. Muhammad, Y. Huang and J. He, *Nanoscale*, 2012, **4**, 2678.
101 W. J. Lee, E. Ramasamy, D. Y. Lee and J. S. Song, *Sol. Energy Mater. Sol. Cells*, 2007, **91**, 1676.
102 Z. S. Wang, Y. Cui, Y. Dan-oh, C. Kasada, A. Shinpo and K. Hara, *J. Phys. Chem. C*, 2008, **112**, 17011.
103 L. H. Hu, S. Y. Dai, J. Weng, S. F. Xiao, Y. F. Sui, Y. Huang, S. H. Chen, F. T. Kong, X. Pan and L. Y. Hu, *J. Phys. Chem. B*, 2007, **111**, 358.
104 S. Q. Bi, F. L. Meng, Y. Z. Zheng, X. Han, X. Tao and J. F. Chen, *J. Power Sources*, 2014, **272**, 485.
105 J. Chen, C. Li, G. Eda, Y. Zhang, W. Lei, M. Chhowalla, W. I. Milne and W. Q. Deng, *Chem. Commun.*, 2011, **47**, 6084.
106 G. Zamiri and S. Bagheri, *J. Colloid Interface Sci.*, 2018, **511**, 318.
107 C. Y. Huang, P. H. Chen, Y. J. Wu, H. P. Chiang, J. S. Hwang, P. T. Lin, K. Y. Lai, F. S. Chien and T. Y. Lin, *Jpn. J. Appl. Phys.*, 2017, **56**, 045201.
108 B. Siwach, D. Mohan and D. Jyoti, *J. Mater. Sci.: Mater. Electron.*, 2017, **28**, 11500.
109 A. Kathalingam, J. K. Rhee and S. H. Han, *Int. J. Energy Res.*, 2014, **38**, 674.
110 F. S. Ghoreishi, V. Ahmadi and M. Samadpour, *J. Power Sources*, 2014, **271**, 195.
111 J. J. Qiu, X. M. Li, F. W. Zhuge, X. Y. Gan, X. D. Gao, W. Z. He, S. J. Park, H. K. Kim and Y. H. Hwang, *Nanotechnology*, 2010, **21**, 195602.
112 J. B. Baxter, A. M. Walker, K. V. Ommering and E. S. Aydil, *Nanotechnology*, 2006, **17**, S304.
113 S. Ameen, M. S. Akhter, M. Song and H. S. Shin, *ACS Appl. Mater. Interfaces*, 2012, **4**, 4405.
114 W. C. Chang, T. C. Tseng, W. C. Yu, Y. Y. Lan and M. D. Ger, *J. Nanosci. Nanotechnol.*, 2016, **16**, 9160.
115 J. L. Song and X. Wang, *Physica E*, 2016, **81**, 14.
116 H. Abdullah, N. A. Atiqah, A. Omar, I. Asshaari, S. Mahalingam, Z. Razali, S. Shaari, J. S. Mandeep and H. Misran, *J. Mater. Sci.: Mater. Electron.*, 2015, **26**, 2263.
117 F. Xu, J. Chen, X. Wu, Y. Zhang, Y. X. Wang, J. Sun, H. C. Bi, W. Lei, Y. Ni and L. T. Sun, *J. Phys. Chem. C*, 2013, **117**, 8619.
118 B. G. Zhai, L. Yang and Y. M. Huang, *Mater. Res. Innovations*, 2015, **19**, s15.
119 G. Khurana, S. Sahoo, S. K. Barik and R. S. Katiyar, *J. Alloys Compd.*, 2013, **578**, 257.
120 Q. H. Chang, Z. J. Ma, J. Z. Wang, Y. Yan, W. Z. Shi, Q. Chen, Y. W. Huang, Q. J. Yu and L. Huang, *Electrochim. Acta*, 2015, **151**, 459.
121 C. E. Small, S. Chen, J. Subbiah, C. M. Amb, S. W. Tsang, T. H. Lai, J. R. Reynolds and F. So, *Nat. Photonics*, 2011, **317**, 115.
122 W. U. Huynh, J. J. Janke and A. P. Alivistatos, *Science*, 2002, **295**, 2425.
123 L. M. Chen, Z. Hong, G. Li and Y. Yang, *Adv. Mater.*, 2009, **21**, 1434.
124 D. Zheng, W. Huang, P. Fan, Y. F. Zheng, J. Huang and J. S. Yu, *ACS Appl. Mater. Interfaces*, 2017, **9**, 4898.
125 B. J. Moon, K. S. Lee, J. Shim, S. Park, S. H. Kim, S. Bae, M. Park, C. L. Lee, W. K. Choi, Y. Yi, J. Y. Hwang and D. I. Son, *Nano Energy*, 2016, **20**, 221.
126 T. Hu, l. Chen, K. Yuan and Y. W. Chen, *Chem. – Eur. J.*, 2014, **20**, 17178.
127 T. Hu, L. Chen, Z. Q. Deng and Y. W. Chen, *J. Mater. Chem. A*, 2015, **3**, 10890.
128 S. R. Gollu, R. Sharma, G. Srinivas, S. Kundu and D. Gupta, *Org. Electron.*, 2016, **29**, 79.
129 A. F. Hu, Q. X. Wang, L. Chen, X. T. Hu, Y. Zhang, Y. F. Wu and Y. W. Chen, *ACS Appl. Mater. Interfaces*, 2015, **7**, 16078.
130 W. J. E. Beek, M. M. Wienk and R. A. J. Janssen, *Adv. Funct. Mater.*, 2006, **16**, 1112.
131 W. J. E. Beek, M. M. Wienk, M. Kemerink, X. N. Yang and R. A. J. Janssen, *J. Phys. Chem. B*, 2005, **109**, 9505.
132 H. Y. Abbasi, A. Habib and M. Tanveer, *J. Alloys Compd.*, 2017, **690**, 21.
133 M. Dutta, S. Sarker, T. Ghosh and D. Basak, *J. Phys. Chem. C*, 2012, **116**, 20127.

 This journal is © The Royal Society of Chemistry 2018

Published on 19 February 2018. Downloaded by HeFei University of Technology on 20/04/2018 03:48:02.

134 K. K. Yang, C. K. Xu, L. W. Huang, L. F. Zou and H. Wang, *Nanotechnology*, 2011, **22**, 405401.
135 Z. Y. Yin, S. X. Wu, X. Z. Zhou, X. Huang, Q. C. Zhang, F. Boey and H. Zhang, *Small*, 2010, **6**, 307.
136 M. Sookhakian, Y. M. Amin, R. Zakaria, S. Baradaran, M. R. Mahmoudian, M. Rezayi, M. T. Tajabadi and W. J. Basirun, *Ind. Eng. Chem. Res.*, 2014, **53**, 14301.
137 R. Sharma, F. Alam, A. K. Sharma, V. Dutta and S. K. Dhawan, *J. Mater. Chem. C*, 2014, **2**, 8142.
138 S. AbdulaAlmohsin and J. B. Cui, *J. Phys. Chem. C*, 2012, **116**, 9433.
139 H. Park, S. Chang, J. Jean, J. J. Cheng, P. T. Araujo, M. S. Wang, M. G. Bawendi, M. S. Dresselhaus, V. Bulović, J. Kong and S. Gradečak, *Nano Lett.*, 2013, **13**, 233.
140 J. Burschka, N. Pellet, S. J. Moon, R. Humphry-Baker, P. Gao, M. K. Nazeeruddin and M. Gratzel, *Nature*, 2013, **499**, 316.
141 H. P. Zhou, Q. Chen, G. Li, S. Luo, T. B. Song, H. S. Duan, Z. R. Hong, Y. S. Liu and Y. Yang, *Science*, 2014, **345**, 542.
142 N. G. Park, M. Grätzel, T. Miyasaka, K. Zhu and K. Emery, *Nat. Energy*, 2016, **1**, 16152.
143 J. H. Qiu, Y. C. Qiu, K. Y. Yan, M. Zhong, C. Mu, H. Yan and S. H. Yang, *Nanoscale*, 2013, **5**, 3245.
144 M. I. Ahmed, Z. Hussain, M. Mujahid, A. N. Khan, S. S. Javaid and A. Habib, *AIP Adv.*, 2016, **6**, 065303.
145 P. S. Chandrasekhar and V. K. Komarala, *RSC Adv.*, 2017, **7**, 28610.
146 W. L. Jiang, W. Zhou, J. F. Ying, T. Y. Yang and Y. M. Gao, *J. Inorg. Mater.*, 2017, **32**, 96.
147 M. M. Tavakoli, R. Tavakoli, Z. Nourbakhsh, A. Waleed, U. S. Virk and Z. Y. Fan, *Adv. Mater. Interfaces*, 2016, **3**, 1500790.
148 K. J. Jiao, X. F. Wu, C. Y. Duan, D. W. Zhang, Y. Wang and Y. F. Chen, *Phys. Chem. Chem. Phys.*, 2015, **17**, 4757.
149 H. Bi, F. Q. Huang, J. Liang, X. M. Xie and M. H. Jiang, *Adv. Mater.*, 2011, **23**, 3202.
150 G. D. Yuan, W. J. Zhang, J. S. Jie, X. Fan, J. A. Zapian, Y. H. Leung, L. B. Luo, P. F. Wang, C. S. Lee and S. T. Lee, *Nano Lett.*, 2008, **8**, 2591.
151 J. G. Lu, Z. Z. Ye, F. Zhuge, Y. J. Zeng, B. H. Zhao and L. P. Zhu, *Appl. Phys. Lett.*, 2004, **85**, 3134.
152 Y. Ye, L. Gan, L. Dai, H. Meng, F. Wei, Y. Dai, Z. J. Shi, B. Yu, X. F. Guo and G. G. Qin, *J. Mater. Chem.*, 2011, **21**, 11760.
153 X. B. Tang, G. M. Li and S. M. Zhou, *Nano Lett.*, 2013, **13**, 5046.
154 K. Chung, C. H. Lee and G. C. Yi, *Science*, 2010, **330**, 655.
155 C. H. Lee, Y. J. Kim, Y. J. Hong, S. R. Jeon, S. Bae, B. H. Hong and G. C. Yi, *Adv. Mater.*, 2011, **23**, 4614.
156 S. G. Zhang, X. W. Zhang, F. T. Si, J. J. Dong, J. X. Wang, X. Liu, Z. G. Yin and H. L. Gao, *Appl. Phys. Lett.*, 2012, **101**, 121104.
157 J. J. Dong, H. Y. Hao, J. Xing, Z. J. Fan and Z. L. Zhang, *Nanoscale Res. Lett.*, 2014, **9**, 630.
158 J. M. Lee, J. Yi, W. W. Lee, H. Y. Jeong, T. Jung, Y. Kim and W. I. Park, *Appl. Phys. Lett.*, 2012, **100**, 061107.
159 W. Z. Liu, W. Wang, H. Y. Xu, X. H. Li, J. G. Ma and Y. C. Liu, *Appl. Phys. Express*, 2015, **8**, 095202.
160 K. Xu, Y. Y. Xie, H. L. Ma, Y. X. Du, F. G. Zeng, P. Ding, Z. Y. Gao, C. Xu and J. Sun, *Solid-State Electron.*, 2016, **126**, 5.
161 D. I. Son, B. W. Kwon, D. H. Park, W. S. Seo, Y. Yi, B. Angadi, C. L. Lee and W. K. Choi, *Nat. Nanotechnol.*, 2012, **71**, 465.
162 H. H. Kim, J. S. Park, I. K. Han, S. O. Won, C. Park, D. K. Hwang and W. K. Choi, *Nanoscale*, 2016, **8**, 19737.
163 K. S. Lee, J. Shim, M. Park, H. Y. Kim and D. I. Son, *Composites, Part B*, 2017, **130**, 70.
164 M. Zubair, M. Mustafa, A. Ali, Y. H. Doh and K. H. Choi, *J. Mater. Sci.: Mater. Electron.*, 2015, **26**, 3344.
165 M. Huang, S. Mao, H. Feick, H. Yan, Y. Wu, H. Kid, E. Weber, R. Russo and P. D. Yang, *Science*, 2001, **292**, 1897.
166 H. Cao, Y. G. Zhao, S. T. Ho, E. W. Seelig, Q. H. Wang and R. P. H. Chang, *Phys. Rev. Lett.*, 1999, **82**, 2278.
167 J. H. Choy, E. S. Jang, J. H. Won, J. H. Chung, D. J. Jang and Y. W. Kim, *Adv. Mater.*, 2003, **15**, 1911.
168 C. Czekalla, C. Sturm, R. Schmidt-Grund, B. Cao, M. Lorenz and M. Grundmann, *Appl. Phys. Lett.*, 2008, **92**, 241102.
169 P. J. Pauzauskie and P. D. Yang, *Mater. Today*, 2006, **9**, 36.
170 D. Y. Lei, J. Li and H. C. Ong, *Appl. Phys. Lett.*, 2007, **91**, 021112.
171 P. R. West, S. Ishii, G. V. Naik, N. K. Emani, V. M. Shalaev and A. Boltasseva, *Laser Photonics Rev.*, 2010, **4**, 795.
172 M. T. Hill, Y. S. Oei, B. Smalbrugge, Y. Zhu, T. D. Vries and P. J. V. Veldhoven, *Nat. Photonics*, 2007, **1**, 589.
173 S. H. Cheng, Y. C. Yeh, M. L. Lu, C. W. Chen and Y. F. Chen, *Opt. Express*, 2012, **20**, 799.
174 J. T. Li, C. X. Xu, H. Y. Nan, M. M. Jiang, G. Y. Gao, Y. Lin, J. Dai, G. Y. Zhu, Z. H. Ni, S. F. Wang and Y. Li, *ACS Appl. Mater. Interfaces*, 2014, **6**, 10469.
175 J. T. Li, M. M. Jiang, C. X. Xu, Y. Y. Wang, Y. Lin, J. F. Lu and Z. L. Shi, *Sci. Rep.*, 2015, **5**, 9263.
176 J. Dai, C. X. Xu, K. Zheng, C. G. Lv and Y. P. Cui, *Appl. Phys. Lett.*, 2009, **95**, 241110.
177 J. T. Li, Y. Lin, J. F. Lu, C. X. Xu, Y. Y. Wang, Z. L. Shi and J. Dai, *ACS Nano*, 2015, **9**, 6794.
178 H. O. Zhu, X. T. Xu, X. Q. Tian, J. N. Tang, H. W. Liang, L. L. Chen, Y. Xie, X. D. Zhang, C. Xiao, R. Li, Q. Gu, P. Hua and S. C. Ruan, *Adv. Mater.*, 2017, **29**, 1604351.